THE FATE OF TERRESTRIAL DISSOLVED ORGANIC MATTER IN OCEAN MARGINS INVESTIGATED THROUGH COUPLED MICROBIAL-PHOTOCHEMICAL INCUBATIONS OF VASCULAR PLANT LEACHATES

A Thesis

by

DANIELLE RENEE CREELEY

Submitted to the Office of Graduate and Professional Studies of
Texas A&M University
in partial fulfillment of the requirements for the degree of

MASTER OF SCIENCE

Chair of Committee,	Karl Kaiser
Committee Members,	Rainer Amon
	Peter Santschi
Head of Department,	Shari Yvon-Lewis

August 2017

Major Subject: Oceanography

ABSTRACT

Rivers are the primary link between terrestrial and marine carbon reservoirs. Dissolved organic matter (DOM) contributes the majority of carbon flux between these environments. Understanding the influence of source, availability and transformations of dissolved organic carbon (DOC) in rivers and coastal ocean systems is important to determine the fate of DOM in the marine environment. Coupled microbial-photochemical incubations were used to analyze microbial and photochemical decomposition of plant leachates and to investigate DOM cycling in the Sacramento-San Joaquin River Delta/San Francisco Bay estuary. A wide range of chemical and optical parameters were tracked during coupled incubations including absorbance, fluorescence, enantiomeric amino acids, and neutral sugars measurements. Vascular plant leachates were characterized by high neutral sugar yields and low amino acid yields with variable THAA and THNS composition. Biomarkers that most accurately tracked vascular plant DOM and microbial DOM during coupled incubations were selected to apply to seasonal transects collected from the Sacramento-San Joaquin River Delta and San Francisco Bay, California. Enantiomeric amino acids and neutral sugars were used to investigate the composition and bioavailability of riverine DOM in this natural system. Biochemical trends in the Delta-Bay system were influenced by source inputs, wetlands, and environmental processes. Differences in DOM composition and concentration related to differences in regions, highlighting heterogenetic inputs, hydrology of the system, and in situ production of DOM. Furthermore, terrestrial DOM was already extensively degraded prior to entering the Delta and was largely refractory throughout the Bay. Neutral sugar yields in the transect were used to determine a median of ~10% terrestrial DOC labile fraction, and amino acid yields were used to determine a median of 5% in situ DOM labile fraction. Median total labile fraction in the Delta and Bay was 21% and was influenced by hydrological conditions in the estuary. Our study demonstrated the complexity of river delta and estuarine systems integrating complex varying sources and decomposition trends connected to seasons and flow regime. Bay systems were

recognized as efficient filters of terrestrial DOM limiting its flux to the ocean and exerting a major control on air-sea CO_2 fluxes, acidification and nutrient budgets in the estuary.

DEDICATION

This work is dedicated to my daughter, Aliera, for her incredible patience with my work and for accompanying the late nights on campus with laughter.

ACKNOWLEDGEMENTS

I would first like to thank my committee chair, Dr. Karl Kaiser, and my committee members, Dr. Rainer Amon and Dr. Peter Santschi, for their support and mentorship and throughout the course of this research. I am grateful to Karl for providing me the opportunity to work on this project and Peter for encouraging me to pursue a master's degree. Furthermore, I am grateful to the National Science Foundation for funding this project and collaborators for help with sample collection and analysis.

I also would like to thank my friends, colleagues, and the department faculty and staff at both College Station campus and Galveston campus for their encouragement and support through the last four years at Texas A&M University. I want to extend a special thanks to Alexandria Rivard and Maria Cañedo Oropeza who helped me navigate grad school and enjoy it!

Finally, I would like to express my unending thanks to my family, especially to Aliera, Aaron, and my mother and father, for their patience, encouragement, and love. Please know of my appreciation for all you have done for me. Thank you for your support.

CONTRIBUTORS AND FUNDING SOURCES

Contributors

This work was supervised by a thesis committee consisting of Dr. Karl Kaiser of the Marine Sciences Department and Oceanography Department, Dr. Rainer Amon of the Marine Sciences Department and Oceanography Department, and Dr. Peter Santschi of the Marine Sciences Department and Oceanography Department.

All work conducted for this thesis was completed by the student independently.

Funding Sources

Graduate study and research was supported by the National Science Foundation award 1333633.

NOMENCLATURE

DOM	Dissolved Organic Matter
DOC	Dissolved Organic Carbon
SF	Soluble Fraction
THAA	Total Hydrolysable Amino Acids
THNS	Total Hydrolysable Neutral Sugars

TABLE OF CONTENTS

Page

LIST OF FIGURES

Page

LIST OF TABLES

1. INTRODUCTION AND LITERATURE REVIEW

Dissolved organic matter (DOM) is an important carbon reservoir in the global carbon cycle. Quantities of DOC in the ocean are of a similar magnitude as CO_2 in the atmosphere, which makes DOM a key carbon reservoir in natural aquatic systems. DOM facilitates about half of the organic carbon flux from terrestrial to marine systems by transport in rivers, and it fuels bacterial and planktonic food webs in riverine and coastal environments.

Rivers serve as important pathways integrating terrestrial carbon stocks with marine carbon reservoirs and estuaries behave as interfaces between them. Estimates of the global dissolved organic carbon (DOC) flux from rivers to the ocean are in the range of 0.20-0.36 PgC per year (Schlesinger and Melack, 1981; Meybeck 1982, 1993; Ludwig et al., 1996; Hedges et al., 1997; Aitkenhead and McDowell, 2000; Cauwet, 2002; Dai et al., 2012). Recent studies find amplified DOC flux from major rivers compared to historic estimates (Frey et al., 2005; Spencer et al., 2009; Holmes et al., 2012). Despite significant inputs of terrestrial DOM from rivers to marine systems, the terrestrial DOM signature in marine systems and DOM is small (Opsahl and Benner, 1997).

River systems and plume waters are very dynamic environments for DOM. In these settings, microbial and photochemical degradation, flocculation and production of autochthonous DOM occurs spurred by availability of nutrients and depth of sunlight penetration (Benner and Opsahl, 2001; Hernes and Benner, 2003). Recent studies have given new knowledge indicating a variety of sources for riverine DOM including vascular plant sources, algal and microbial contributions and non-vascular plant sources such as mosses (Hernes et al., 2007; Burns et al., 2008; Kraus et al., 2008; Spencer et al., 2008). DOM bioavailability in riverine and estuarine systems ranges from labile to refractory, but DOM is heavily degraded before it leaves the coastal shelves (Cauwet, 2002; Bianchi et al., 2004; Zou et al., 2004).

Given all uncertainties related to sources and transformations of DOM in river and estuarine systems, efforts are needed to establish quantitative tools for determination of degradation and production rates toward a better understanding of ecosystem functioning. The objective of this study is to develop and calibrate DOM source biomarkers for vascular plant and microbial sources using plant leachates and apply these to study DOM processing in the Sacramento/San Joaquin River Delta and San Francisco Bay estuary.

1.1 Sources and Transformations of Riverine DOM

DOM composition is shaped by its original source, environmental conditions, and processing via photochemical and biodegradation pathways. Important sources of riverine DOM are runoff from soils, groundwater, atmospheric inputs, and in situ production (phytoplankton and microbial activity). Soil-derived DOM constitutes an important component of riverine DOM. Leaching of soil organic matter (SOM) enables mobilization of DOM through watersheds via streams and groundwater. DOM from soils is derived from fresh plant material and humic substances, which provide an abundance of senescent plant and microbial biomass. Contributions to riverine DOM through atmospheric input are still quantitatively unknown. However, the flux of atmospheric DOM to riverine DOM has been suggested to be significant.

Prokaryotic organisms, specifically bacteria, are considered to be the essential engines of transformation reactions of DOM. Recent research also suggests aquatic fungi play a substantial role in the decomposition of DOM in aquatic ecosystems. Terrestrial fungal communities are in litter input from leaves, flowers, and wood as well as in soil and play a major role in soil biogenesis (Dighton and Boddy, 1989). Aquatic fungal communities are prominent in aquatic systems with high vegetation coverage and dissolved nutrients such as coastal waterways, marshlands, swamps, and streams. Fungal metabolic recycling of emergent wetlands plants in these systems contributes significant cycling of nutrients and energy (Newel, 1993; Newell and Porter, 2000). Fungal species

are selective in the organic matter compounds they decompose due to the types of enzymes they utilize (Sinsabaugh and Liptak, 1997; Said-Pullicino et al., 2006).

Microbial transformations and contributions to the riverine DOM pool can occur in several stages of the DOM flux from land to ocean margins. Microbial degradation of leached organic matter in soils can lead to altered, highly labile DOM pools (Williams and Edwards, 1993). Autochthonous contributions are another component to riverine DOM through algal blooms that can occur during low flow seasons like late summer and early fall (Raymond and Bauer, 2001; Royer and David, 2005; Roach 2013).

The dynamic environment of aquatic systems such as rivers enables transformations of DOM through photochemical and microbial processes. Photochemical processing of molecules occurs during exposure to irradiation. Microbial processing occurs from the enzymatic reworking of molecules by organisms such as bacteria. Both photochemical and microbial processes decompose, cycle, transform and remineralize dissolved organic carbon (DOC) in aquatic environments. The extent of phototransformation is dependent on the composition of the DOM and exposure to solar radiation. Furthermore, riverine DOM composition and signature can be impacted by river discharge rates through increased water runoff, litter leaching, and residence time leading to more material input with less time for microbial and photochemical degradation (Boyer et al., 1997; McGlynn and McDonnell, 2003).

Microbial and photochemical processes coupled in the environment decompose more DOC than either individually (Miller and Moran, 1997; Mopper and Kieber, 2002; Obernosterer and Benner, 2004; Fichot and Benner, 2014). Fichot and Benner (2014) determined that while direct photomineralization alone contributed to minor amounts (~6%) of mineralization of annual tDOC discharged from the Mississippi-Atchafalaya River to the Louisiana shelf, biomineralization accounted for the vast majority (~94%) of mineralization. Fichot and Benner (2014) results suggest biomineralization of tDOC in the mixed layer was augmented ~50% by photochemical transformations. However, it has been reported there is potential in small artic rivers for photochemical degradation to

play a more important role than enhancing microbial degradation of DOM (Cory et al., 2014).

Degradation-resistant DOM is delivered to marine environments after transformations and extensive degradation in these riverine systems (Druffel et al., 1992; Opsahl and Benner, 1998; Loh et al., 2004; Dittmar and Paeng, 2009). Recent analysis using FT-ICR-MS on riverine DOM demonstrated a shift from a terrestrial signature to marine signature caused by photochemical effects (Stubbins et al., 2010). The rapidity of photodegradation of DOM and reworking of DOM into degradation-resistant material on spans of time from days to decades gives it a unique opportunity to be both a carbon source and sink (Druffel et al., 1992; Loh et al., 2004; Dittmar and Paeng, 2009). Photochemical alterations of terrestrial DOM can degrade high-molecular weight (HMW) compounds, producing low molecular weight (LMW) photo-degradation resistant compounds that are bio-labile (Mopper and Stahovec, 1986; Mopper et al., 1991; Opsahl and Benner 1998; Mopper and Kieber 2002). Furthermore, diagenetic processes work DOM into smaller components that are less bioavailable and with decreasing molecular size, bioreactivity decreases (Kaiser and Benner, 2009). Microbial alterations of riverine DOM occur alongside photochemical processes and can be enhanced by photochemical effects (Fichot and Benner, 2014). DOM composition contains amino acids and carbohydrates that are bioavailable components that fuel microbial reworking of DOM and produce pools of labile microbial DOM. This processing of DOM demonstrates the importance of DOM in biogeochemical cycling from terrestrial carbon reservoirs to marine carbon reservoirs.

Understanding DOM's reprocessing and transformations during riverine transport to marine systems is important in furthering understanding of the global carbon cycle as well as the role of DOM in the global carbon cycle. DOM reactivity and bioavailability, which is influenced by source, determines the extent of transformation and reprocessing (Hedges, 1992, Hedges et al., 1997). Furthermore, the composition of the DOM plays a large role in the extent of its bioavailability and degradation. Characteristics such as absorbance, amino acid composition, and carbohydrate

composition determine the extent of degradation both from photochemical and microbial processes (Opsahl and Benner, 1998; Osburn et al., 2001; Carlson and Hansell, 2014; Mannino and Harvey, 2000).

1.2 Biochemical and Optical Indicators of Riverine DOM

Characterization of DOM has been done using bulk properties such as dissolved organic carbon (DOC), isotopic compositions, optical properties including chromophoric dissolved organic matter (CDOM) absorbance and fluorescence, and chemical biomarkers such as amino acids and carbohydrates.

In part, terrestrial DOM is composed of vascular plant material. Vascular plants have unique structural characteristics that can be utilized as biomarkers. Biomarkers, unique characteristics used as indicators for a source or process, are useful tools to qualitatively determine the composition of DOM. Terrestrially derived DOM has a higher aromaticity compared to microbial DOM (Sleighter and Hatcher, 2008). Photochemical degradation preferentially removes or alters key components of terrestrial material such as CDOM (Opsahl and Benner, 1998; Hernes and Benner, 2003; Benner and Kaiser, 2011). Increased solar exposure causes CDOM abundance to decrease through photochemical degradation as CDOM absorbs high-energy light (Miller and Zepp, 1995; Helms et al., 2013).

The optical properties of terrestrially derived CDOM differ significantly to marine CDOM (Coble, 2007; Fellman et al., 2010). Spectral slope (S) values for coastal CDOM at wavelength 300-600 nm range from 15 to 19 μm^{-1} (Stedmon et al., 2011). UV slope values from wavelength 275-295 ($S_{275-295}$) normally fall between 10 to 20 μm^{-1} for terrestrially derived material (Helms et al. 2008; Fichot and Benner, 2012). Marine CDOM signatures have higher S values of about 20 to 30 μm^{-1} (Stedmon et al., 2011). The specific absorbance of UV at wavelength 254 nm, known as $SUVA_{254}$, is another optical property used to distinguish DOM source. Higher $SUVA_{254}$ values show a larger terrestrial signature (Neff et al., 2006; Jaffe et al., 2008).

Fluorescence spectroscopy can be utilized to analyze DOM using an excitation-emission matrix (EEM). EEM is a highly sensitive spectroscopy used to determine the origin of DOM (Mopper and Schultz, 1993; Cory and McKnight, 2005; Coble, 2007). The fluorescence index, a ratio of emission intensity at wavelengths 450 nm and 500 nm at excitation 370 nm, can be used to distinguish DOM sources (McKnight et al., 2001). An increase in the fluorescence index value is attributed to increased microbial contribution to DOM (McKnight et al., 2001; Cory and McKnight, 2005). This index is useful for determining DOM sources, but cannot be applied in plume waters to accurately distinguish between microbial or photochemically degraded sources due to a similar CDOM signature (Moran et al., 2000; Spencer et al., 2009).

Carbohydrates are compounds of polyhydroxyl aldehydes and ketones that form the structural and storage components of both terrestrial and aquatic organisms and are the most abundant major component in vascular plants (~75% weight) (Aspinall, 1970; Aspinall, 1983; Bianchi and Canuel, 2011). The dominant structural polysaccharides of vascular plants, cellulose and hemicellulose, are composed of carbohydrates, made up partially by neutral sugars (fucose, rhamnose, ribose, arabinose, galactose, glucose, mannose, xylose, and lyxose) (Aspinall, 1983). Due to this prevalence of neutral sugars in cellulose, a component of plant cell walls, analysis of neutral sugars in DOM is important (Opsahl and Benner, 1999). Determining the abundance of individual neutral sugars in DOM can be applied to distinguish sources (Cowie and Hedges, 1984), and quantification of total hydrolysable neutral sugars (THNS) can augment carbon fluxes between carbon reservoirs. Furthermore, THNS yields can be applied as a useful index of DOM degradation with higher yields determining fresher, bioavailable material and lower yields indicating degradation (Cowie and Hedges, 1994; Skoog and Benner, 1997; Amon et al., 2001). Amon and Benner (2003) used neutral sugar yields (% OC) to quantitatively determine the amount of labile DOM in the Arctic Mediterranean Sea. Glucose is an important neutral sugar in cellulose of vascular plants, and glucose and xylose abundance can be treated as an index of DOM lability (Opsahl and Benner, 1993, 1999; Amon et al., 2001; Amon and Benner, 2003). Increased fucose concentrations are

indicative of being bacteria or phytoplankton derived and high contributions of ribose, mannose, and galactose can be derived from microorganisms (Aspinall, 1983; Moers and Larter, 1993). There is potential to use deoxy sugars as an indicator of highly degraded plant material (Hedges et al., 1994; Opsahl and Benner, 1999), but deoxy sugar concentrations can include contributions from microbial biomass as well (Cowie and Hedges, 1984).

Proteins are important macromolecules built from chains of amino acids linked by peptide bonds that compose a significant portion of labile DOM. Proteins are composed of 20 different α-amino acids with varying functional groups. Amino acid molar abundance can be a useful tool to determine decomposition of DOM (Cowie and Hedges, 1994; Dauwe and Middleburg, 1998). D-enantiomers of amino acids (D-AA) are unique amino acids found only in bacterial macromolecules and indicative of a bacterial signature with increasing abundance of the D form (Dittmar et al., 2001; Perez et al., 2003; Kaiser and Benner 2008; Tremblay and Benner, 2009). Total hydrolysable amino acid (THAA) yields can be applied as a useful index of DOM degradation with higher yields determining fresher, bioavailable material and lower yields indicating degradation (Cowie and Hedges, 1994; Benner and Kaiser, 2003).

1.3 Characteristics of the Sacramento/San Joaquin River Delta and San Francisco Bay Estuary

Estuaries are aquatic systems that link rivers to the coastal ocean. The San Francisco Bay estuary is the system that connects the Sacramento-San Joaquin River Delta to the Pacific Ocean. The Delta is primarily marshland with over 50 islands and tracts, most of which are below sea level and protected from flooding by over 1000 miles of levees (Ingebritsen et al., 2000). Figure 1 developed by California's Department of Water Resources details the varying complexities of the Sacramento-San Joaquin River Delta system. The San Francisco Bay estuary is a tidal-influenced environment. During low inflow of freshwater from the Delta, higher salinity water from the Pacific is

drawn into the Bay and Delta. Increased draw from upstream freshwater causes less outflow to the Bay and further tidal flow through the Delta and upstream.

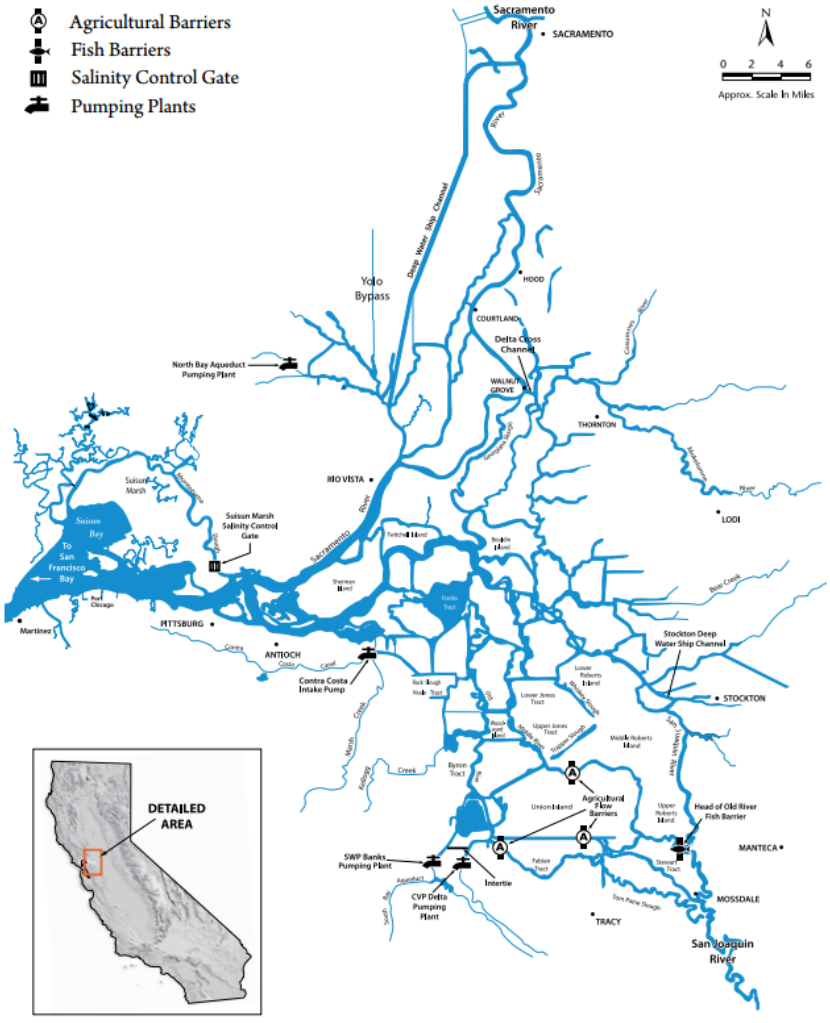

Figure 1 Detailed layout of the Sacramento-San Joaquin River Delta, California with large anthropogenic structures marked (reprinted from Healey et al., 2008).

The Sacramento-San Joaquin Rivers feed ~100 m^3s^{-1} of water to the San Francisco Bay estuary during seasonal low inflow, typically in the summer and autumn. During large flood events, inflow from the rivers can be >9000 m^3s^{-1} (Cloern and

Dufford, 2005). Using flow data from 1980-1991, California's Department of Water Resources (1993) determined the Sacramento River streamflow delivered 829 m^3s^{-1} inflow to the delta annually, while the San Joaquin delivered 168 m^3s^{-1} to the delta annually, and the outflow to the San Francisco Bay was 821 m^3s^{-1} annually. In 2000, the URS Corporation (2007) reported an average inflow from the San Joaquin as 111 m^3s^{-1} of water to the Delta, and 832 m^3s^{-1} from the Sacramento River to the Delta. Outflow to the Bay was an average 710 m^3s^{-1} (Figure 2). Outflow of riverine discharge from the Delta to the Bay has been in decline due to factors including prolonged drought and increased water usage.

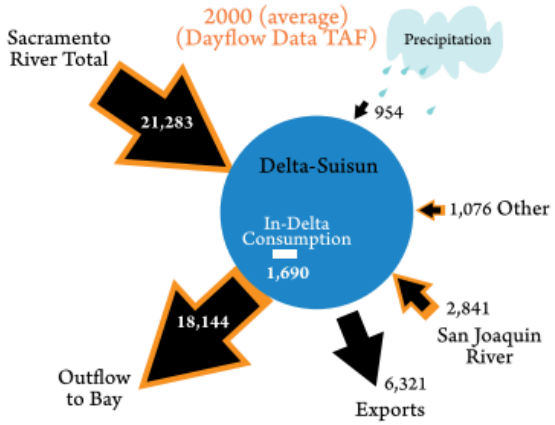

Figure 2 Average water flux into the Delta and out to the bay through river inflow and precipitation, and export before outflow using thousand acre-feet in 2000 (reprinted from URS Corporation, 2007).

Problems the Delta and Bay currently face include water quality impacted by land use (agriculture and urban use and collapsing levees), water discharge (diversion of upstream freshwater inflow and highway and urban water runoff), changing hydrology (encroaching tidal water further upstream and channel dredging for shipping lanes), and rising sea levels. While the Delta is an important source of water for California (URS Corporation, 2007), the Delta-Bay is an important area for agriculture and shipping

transport as well. Following the Gold Rush and the resulting increased demands for food, the Delta's natural levees were raised to repurpose the surrounding marshlands for agricultural purposes (Healey et al., 2008). Agricultural land use acts as an organic matter reservoir, and the agricultural land around the Delta is irrigated using water drawn from the Delta itself. Some of the reclaimed wetland available after construction of the levees is used as diked wetlands in the form of salt ponds and storage or treatment ponds. Treatment ponds contain runoff for treatment before it reenters the Delta-Bay, while contaminants settle and are dredged from these ponds later (Healey et al., 2008). Networks of drainage ditches and pumps are used to lower groundwater tables to prevent flooding of these reclaimed areas (Figure 3).

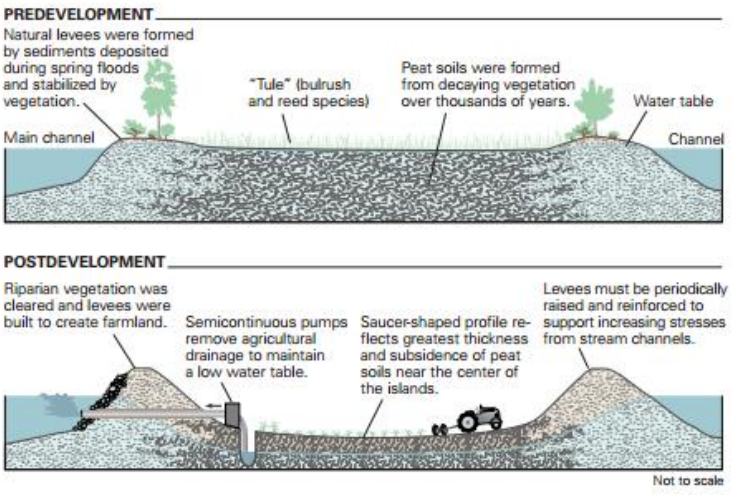

Figure 3 Illustration of an agricultural island below sea level in the Delta demonstrating the use of a pump to prevent internal flooding from groundwater (reprinted from Ingebritsen et al., 2000).

The land surrounding the Delta-Bay is used not only for agricultural purposes but industrial. The industry along the Delta is supported with shipping through the Delta. There are two seaports in the Delta: Sacramento and Stockton. To facilitate shipping transportation, channels were dredged through the Bay to the Delta to connect the ports

(Healey et al., 2008). Furthermore, the Delta is crossed with major roadways and serves as a recreational area for water sports such as boating and swimming as well as commercial fisheries.

DOM impacts the bioavailability and solubility of trace metals and organic contaminants (Santschi et al., 1997; Gourlay et al., 2005; Fukushima et al., 2006). In the past, fish poisonings in the Bay occurred due to selenium in oil refining and soil irrigated in San Joaquin Valley. Selenium contamination from agricultural runoff and naturally occurring mercury as well as mercury released by the Gold Rush are still present contaminants in the Delta-Bay today and can be remobilized from the sediments of the bay (Healey et al., 2008). Dredging of the channels to keep shipping lanes open through the Delta resuspend sediments, which can cause mobilization of contaminants. These contaminants present a danger to both public and environmental welfare and further highlight the importance of DOM in this system.

1.4 Experimental Objectives

Current knowledge of riverine and plume DOM sources is largely qualitative. Without quantification of riverine and plume DOM sources, the ability to calculate fluxes of either photo-labile or bio-labile DOM to marine systems that are reactive on timescales relevant to coastal processes is unavailable. Determining the fate and accurately quantifying the flux of DOM from terrestrial to marine environments will increase understanding of the global carbon cycle and riverine DOM's role in such (Hedges, Keil, & Benner, 1997). While incubation experiments have been done for both microbial and photochemical degradation individually to help further understanding, Fichot and Benner (2014) showed the most comprehensive study for in situ degradation within riverine systems. This previous work suggests a coupled incubation will more accurately reflect DOM-signatures collected from marine environments.

Using this approach, one objective of this research was to determine which molecular biomarkers reflect the bioavailability and transformations of terrigenous DOM by microbial and photochemical processes in bioassay experiments. To test this, coupled

photochemical-microbial incubation experiments with controlled light exposure and known spectral irradiation were utilized to more accurately reflect DOM removal processes in riverine and coastal systems. Analysis of amino acids and carbohydrates developed and calibrated DOM source biomarkers for vascular plants and microbial sources.

The second objective of this research was to apply calibrated biomarkers to describe DOM transformations across the salinity gradient in the San Francisco Bay estuary during winter and summer. From determining DOM source biomarkers for vascular plant and microbial sources, these carbon-normalized biomarkers can be used to study degradation and production of DOM in riverine and estuarine environments. The carbon-normalized biomarkers were applied to the Sacramento-San Joaquin River Delta/San Francisco Bay estuary in California.

2. METHODS

Rivers serve as important pathways linking terrestrial carbon stocks with marine carbon reservoirs, and estuaries behave as interfaces between them. This flux of DOM through rivers is a major source of reduced carbon for aquatic and marine environments. Estimates of the global dissolved organic carbon (DOC) flux from rivers to the ocean are in the range of 0.20 to 0.36 PgC per year (Schlesinger and Melack, 1981; Meybeck 1982, 1993; Ludwig et al., 1996; Hedges et al., 1997; Aitkenhead and McDowell, 2000; Cauwet, 2002; Dai et al., 2012).

Riverine DOM is derived from multiple sources including soil leachates, agricultural, industrial and urban surface runoff, groundwater, atmospheric inputs, and in situ production (phytoplankton and microbial activity). The dynamic environment of aquatic systems such as rivers enables transformations of DOM through photochemical and microbial processes. Riverine DOM is an important fuel for microbial communities in estuarine and coastal systems and also undergoes flocculation, adsorption, and degradation through microbial and photochemical processes. Each of these factors can impact the concentrations of DOC and composition of DOM delivered to marine environments by rivers.

The Sacramento-San Joaquin River Delta receives approximately 35 x 10^9 m^3 $year^{-1}$ freshwater input from the Sacramento and San Joaquin River and is the greatest source of terrestrial DOM in the Delta (Paulsen, 1997). Residence times ranging from a couple weeks to over a month in the Sacramento River and San Joaquin River to Suisun Bay enable microbial and photochemical transformations that alter and/or degrade the terrestrial DOM before it enters the Bay and ultimately the marine environment (Sommer et al., 2006).

Recent studies increasingly find larger estimates of DOC flux from major rivers compared to historic estimates (Spencer et al., 2009; Holmes et al., 2012). Understanding the effect of origin and transformation processes on riverine DOM will

help predict the fate of DOM in ocean margins and gain a better understanding of DOM fate with these increasing fluxes.

2.1 Coupled Photochemical-Microbial Incubations

For coupled incubations, vascular plant material leachates were prepared with five different plant materials collected from the Sacramento River Valley and estuarine wetlands (obtained from the Sierra Foothills Research and Extension Center in California and from Sacramento River/San Joaquin River Delta wetlands): gymnosperm needles from *Pinus sabiniana* (foothill pine), angiosperm dicot leaves from *Quercus douglassi* (blue oak), angiosperm monocot mixed annual grasses, angiosperm monocot mixed *Schoenoplectus acutus* (tule), and *Typha latifolia* (cattails) (Table 1). Collected plant samples were oven dried and ground to pass through a 350-µm sieve.

About 5 - 7 g of dried plant litter were mixed and leached in 2.5 L of pure Milli-Q water and mixed during the following 24 hour. After 24 hours of leaching, 2.5 L of UV-oxidized deep Gulf of Mexico water was mixed with the leached sample then filtered through a 0.2µm (Whatman Polycap 75 AS). Following filtering, aliquots of the vascular plant leachate were collected into labeled, precombusted vials for analysis of optical properties, DOC, and biochemical analysis in the initial vascular plant DOM. These initial samples were called t0.

Table 1 Dominating vegetation from the study site chosen for coupled incubation experiments and the number of samples resulting from incubations of leachates.

Incubations	Samples
Angiosperm mixed monocot grasses	6
Typha latifolia (cattails)	6
Pinus sabiniana (foothill pine)	6
Schoenoplectus acutus (tule)	6
Quercus douglassi (blue oak)	5

After sampling t0, 100 mL of inoculum collected from Shell Beach in Galveston was added to the remaining leachate and mixed well to introduce microbial communities. Then the leachate was separated into five quartz flasks and stored in the dark. Photooxidation occurred at 400 W m^{-2} irradiance (noontime irradiation) on a 5 hr-light/19 hr-dark cycle in a Suntest XLS (Xenon lamp) while kept cool in a 19°C water bath during photo oxidation to regulate incubation temperature. After photo oxidation, the samples were shaken to mix, aerated using a piece of 450°C combusted glass tubing, and stored in the dark for microbial incubations.

Six time points were collected at spaced stages of degradation. Each time point was filtered through a 450°C combusted 0.45 µM GF/F filter to remove particles. Aliquots of the filtrate was stored for optical, DOC, and biochemical analyses.

2.2 Transect Sample Collection

Samples were collected in transects of the Sacramento-San Joaquin River Delta through the San Francisco Bay Estuary to the mouth of the river during the winter season in 2014 and summer seasons in 2015 and 2016 (Fig. 4). Stations were chosen based on ranging salinity, with the Golden Gate Bridge (marine endmember), Vernalis (San Joaquin River endmember), Garcia Bend (Sacramento River endmember), and Belden's Landing sampled at every transect. Surface water was collected at each station using an in-situ pump, filtered through a 0.2 µm Whatman capsule filter to remove particles and stored in 60 mL HDPE Nalgene bottles. Samples were stored frozen except an aliquot stored in the refrigerator for optical analyses.

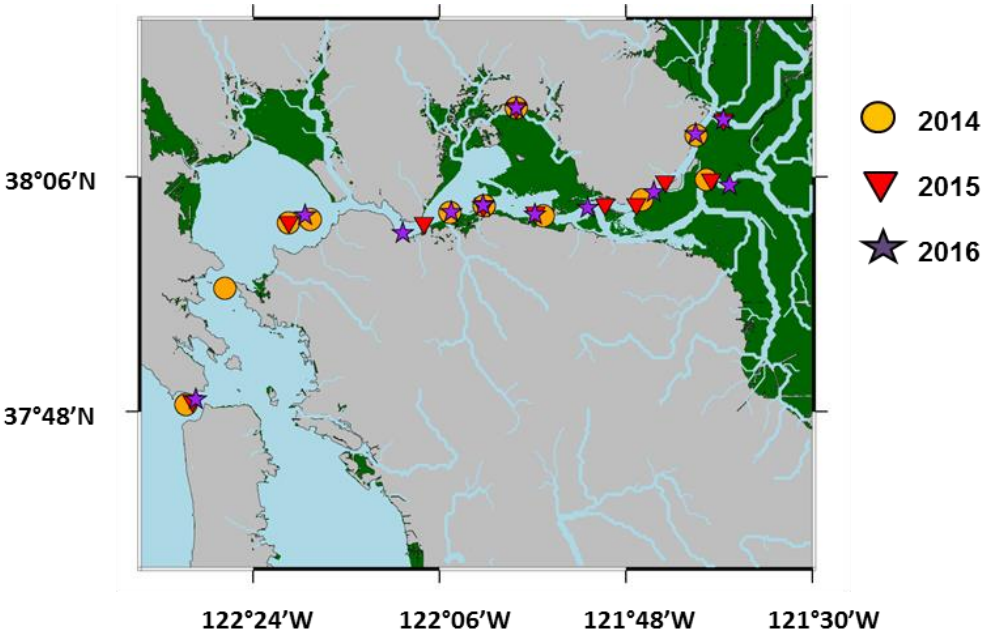

Figure 4 Study site showing the sampling stations for 2014, 2015, and 2016 in San Francisco Bay Estuary and Sacramento-San Joaquin River Delta in California.

2.3 Dissolved Organic Carbon (DOC)

Dissolved organic carbon was measured by a high-temperature combustion method according to Benner and Strom, 1994. The system used was a Shimadzu TOC-V system with autosampler. Calibration was performed with potassium hydrogen phthalate and each sample was measured four times.

2.4 Absorption Measurements and Calculations

Absorbance scans between 200-800 nm were acquired in 1 cm quartz cuvettes using a Shimadzu UV -1800 spectrophotometer. The absorbance spectra were corrected using an exponential fit of the absorbance data and a calculation of the offset value and subtracting that from the spectrum (Fichot and Benner, 2011; Fichot et al., 2014; Kaiser et al., 2016). The Naperian absorption coefficient (a_g (λ) m^{-1}) at 254 nm was calculated with the corrected absorbance data and the equation from Helms et al. (2008):

$$a = 2.303\, A/l$$

where A is the absorbance and l is the path length (m).

The spectral range between 275-295 nm and 350-400 nm were log-linearized $a_g(\lambda)$ before applying a linear fit to calculate the spectral slope coefficient. The slope ratio (S_R) was determined using the ratio of the spectral slope coefficient of 275-295 nm ($S_{275-295}$) and the coefficient for 350-400 nm ($S_{350-400}$) (Helms et al., 2008). $SUVA_{254}$ (L mgC^{-1} m^{-1}) was calculated by dividing UV-absorbance at wavelength 254 nm with the DOC concentration (Weishaar et al., 2003). DOC aromaticity was calculated according to Weishaar et al. (2003) using the following equation:

$$Aromaticity\ (\%\ OC) = 6.52(SUVA_{254}) + 3.63$$

Fichot et al. (2016) developed two empirical models to calculate dissolved lignin phenols ($TDLP_9$) using the relationship between lignin and CDOM. These two models were applied to the transect samples collected in 2014, 2015, and 2016 to determine $TDLP_9$ concentrations. The first model was applied to samples with a Naperian absorption coefficient at wavelength 250nm ($a_g(250) < 4\ m^{-1}$as follows:

$$\ln(TDLP_9) = 0.7672 \times a_g(263) - 0.3987$$

The second model calculated $TDLP_9$ of samples with $a_g(250) > 4\ m^{-1}$as follows:

$$\ln TDLP_9 = -2.282 \times \ln\left(a_g(350)\right) - 8.209 \times \ln\left(a_g(275)\right) + 11.365 \times \ln\left(a_g(295)\right) + 2.909$$

2.5 Chromophoric Dissolved Organic Matter (CDOM) Fluorescence

Fluorescence scans for CDOM were collected using a Photon Technology International, QuantaMaster 4SE Spectofluorometer collecting an excitation/emission (EEM) scan in 5nm increments at excitation from 220-450 nm and emission from 280-600 nm. Samples were analyzed in quartz cells using the fluorescence indices in Table 2. The fluorescence index (FI) uses the optical properties of DOM to distinguish terrestrial

versus microbial sources (McKnight et al., 2001; Cory and McKnight, 2005). This index was modified by Cory and McKnight (2005) as the ratio of emission wavelengths at 470 nm and 520 nm at excitation 370 nm. The humification index (HIX) determines the extent of humification using the ratio of emission from area 435-480 nm and the combined area from 300-345 nm and 435-480 nm at excitation 254nm (Ohno, 2002). The biological/autochthonous index (BIX) is applied to determine the contribution of microbially transformed DOM (Huguet et al., 2009; Walker et al., 2013). BIX was calculated using the ratio of emission at 380 nm and 430 nm at excitation 310 nm (Huguet et al., 2009).

2.6 Total Hydrolysable Neutral Sugars (THNS)

Concentrations of Fucose (Fuc), Rhamnose (Rha), Arabinose (Ara), Galactose (Gal), Glucose (Glc), Mannose (Man), and Xylose (Xyl) were analyzed high-performance anion-exchange chromatography on a Dionex 500 system coupled to a pulsed amperometric detector (PAD) following the method provided by Skoog and Benner (1997) with modifications by Kaiser and Benner (2005). Deoxyribose was used as an internal standard. A self-absorbed ion retardation resin was used to neutralized water samples after hydrolysis in 1.2 M H_2SO_4 (5 h, 100 °C). Samples were desalted and purified by solid-phase extraction using a 50:50 mixture of Biorad's AG50 X8 resin in the H^+-form and AG2X8 resin in the $HCO3^-$-form before chromatographic analyses.

Table 2 Calculations and descriptions for applied fluorescence indices.

Parameter	Calculation	Description
Fluorescence Index (FI)	At ex 370nm, the ratio of em 470nm and 520 nm	Uses optical properties of DOM to distinguish between terrestrial and microbial sources (McKnight et al., 2001; Cory and McKnight, 2005).
Humification Index (HIX)	At ex 254nm, the ratio of em from area 435-480 nm and the combined area from 300-345 nm and 435-480 nm	Ohno's (2002) modified calculation of Zsolnay et al.'s (1999) HIX indicates the degree of humification in DOM
Biological/autochthonous index (BIX)	At ex 310nm, the ratio of em 380nm and 430nm	Applied to determine the contribution of microbially transformed DOM (Huguet et al., 2009; Walker et al., 2013)

2.7 D/L Amino Acids (DLAA)

Aspartic acid (Asx), glutamic acid (Glx), serine (Ser), histidine (His), glycine (Gly), threonine (Thr), arginine (Arg), alanine (Ala), tyrosine (Tyr), valine (Val), phenylalanine (Phe), isoleucine (Ile), leucine (Leu), and lysine (Lys) enantiomers were analyzed using an Agilent 1260 Infinity HPLC system coupled with a fluorescence detector following the methods developed by Kaiser and Benner (2005). Water samples were hydrolyzed at 110°C in a GC oven using 6 M hydrochloric acid for twenty hours and dried down using ultra high purity nitrogen gas. After neutralization samples were redissolved in 0.01 mol L^{-1} borate buffer (pH=9.6), free-amino-acid enantiomers were derivatized with a mixture of N-isobutyryl-L-cysteine (IBLC) and o-phthaldialdehyde (OPA) and separated on a reversed-phase Poroshell 120 EC-C-18, 4.6x100mm, 2.7 micron using mobile phases of 40mM K_2HPO_4 aqueous buffer at pH 6.12 and a 30:1 organic solution of methanol:acetonitrile. Measured values of enantiomeric amino acids

were corrected for acid-catalyzed racemization using the mean of the racemization observed in proteins and free amino acids (Kaiser and Benner, 2005).

2.8 Calculation of Biolabile DOC in Delta and Bay Samples

The labile fractions of DOC in transect samples were calculated using the equations developed by Davis and Benner (2007):

$$(L+S)_y = \left(L_f \times L_y\right) + (S_f \times S_y)$$

$$L_f + S_f = 1$$

These equations were applied to the amino acid yields and neutral sugar yields in the transects to determine the labile in situ DOC and the terrestrial DOC (tDOC) respectively. The labile fraction of in situ DOC was calculated using labile, semi-labile, and refractory yields of amino acids provided by Davis and Benner (2007), where L_y was 21%, S_y was 1.2%, and $(L + S)_y$ was calculated by subtracting the provided refractory THAA yield (0.7%) from the THAA yield measured in the transect sample. The second equation was rearranged to solve for S_f. The final equation for labile fraction of in situ DOC was:

$$(THAA\ Yield - 0.7\%) = \left(L_f \times 21\%\right) + ((1 - L_f) \times 1.2\%)$$

The labile fraction of terrestrial DOC was calculated using labile, semi-labile, and refractory yields of neutral sugars generated from our incubation experiments, where L_y was the average of the labile yield in leachates (16.85%), S_y was the average of the semi-labile yield (1.93%), and $(L + S)_y$ was calculated by subtracting the truly refractory THNS yield (0.4%) from the THNS yield measured in the transect sample. The second equation was rearranged to solve for S_f. The final equation for labile fraction of terrestrial DOC was:

$$(THNS\ Yield - 0.4\%) = \left(L_f \times 16.85\%\right) + ((1 - L_f) \times 1.93\%)$$

Labile DOC for the purpose of this thesis is on the time scale of days to weeks (~14 days).

3. RESULTS

3.1 Initial Composition of Leachates

All litter types used in incubations had organic carbon contents between 39-48% and organic nitrogen contents < 1% (Table 3). The carbon/nitrogen (C/N) atomic ratios ranged from 54 to 117, and the C/N ratio was lowest in oak and mixed grasses and highest in cattails and tule (Table 3). Oak litter had over 25% soluble organic carbon during the described leaching conditions compared to pine litter with ~12% followed by mixed grasses, tule, and cattails at only ~3-4% of available litter organic carbon (Table 3). Initial THAA yields ranged from 0.6 to 4.1 % OC in litter leachates (Table 3). Litter leachates had THNS yields in the range of 8.4 to 16.9 % OC. The cattails leachate had a lower THNS yield (4-8% OC) than other litter leachates. Mixed grasses leachates yielded the highest THAA yield, and pine and mixed grasses litters yielded the highest THNS yields (Table 3). About 27-35% of the soluble fraction was composed of THAA, THNS, and aromatic compounds (%). Cattail and oak leachates had the highest aromaticity at 18.6 % and 21.6 % OC, respectively, while pine leachate had the lowest aromaticity at 9.7 % OC (Table 3).

Table 3 Weight percent carbon per litter, weight percent nitrogen per litter, soluble fraction (SF) yield, total hydrolysable amino acid (THAA) carbon-normalized yield, total hydrolysable neutral sugar (THNS) carbon-normalized yield, and aromatic carbon percentage per litter type.

Litter Type	Litter			Leachate			
	Wt % C	Wt % N	C/N[a]	SF[b] (% OC)	THAA[c] (% OC)	THNS[c] (% OC)	% Aromaticity[d]
Mixed Grasses	39	0.76	60	4.4	4.1	16.3	12.9
Cattail (*Typha latifolia*)	41.6	0.41	117	3.6	2.0	8.4	18.6
Pine (*Pinus ponderosa*)	47.9	0.77	73	12.2	0.6	16.9	9.7
Tule (*Schoenoplectus acutus*)	40.4	0.43	110	3.7	1.2	14.9	16.4
Oak (*Quercus douglassi*)	44.7	0.97	54	25.8	0.7	12.8	21.6

[a] Carbon/nitrogen atomic ratio
[b] The soluble fraction (SF) of carbon in the litter
[c] Total hydrolysable amino acid (THAA) yield and total hydrolysable neutral sugar (THNS) yield calculated as a percentage of DOC
[d] Aromaticity calculated using the relationship to $SUVA_{254}$ described by Weishaar et al. (2003) using the equation: Aromaticity (%OC) = $6.52(SUVA_{254}) + 3.63$

3.2 Molecular and Chemical Changes during Leachate Decomposition

Optical proxies and biochemical analyses measured during incubations are summarized in Table 4. Initial concentrations of DOC in vascular plant leachates ranged from 1242 to 9606 µmol L^{-1} (Table 4). DOC concentrations in all vascular plant leachates decreased over time during incubations, and ending concentrations of DOC in all leachates ranged from 314 to 3162 µmol L^{-1} (Table 4, Figure 5). Grasses leachate had the greatest loss of DOC concentration over the course of the incubation, and DOC (% of initial) decreased most rapidly in grasses between early time points than other leachate types. Cattails leachate had the most gradual change in DOC across time points and the smallest loss of DOC concentration (Table 4, Figure 5).

The concentration of THNS to the initial (% Initial) decreased for all leachate types over time with a loss of 40% of the initial THNS before the first 20 days of the coupled incubations (Figure 5). In tule, 98% THNS (% Initial) was removed during the coupled incubations while cattails had 60% removed (Figure 5). The concentration of THAA (% Initial) decreased for all leachate types over time (Figure 5). Grasses' THAA (% Initial) ~80% by the first two days of the coupled incubation.

Table 4 DOC concentrations, optical absorption, and fluorescence absorption were analyzed for each time point in all coupled incubations. Concentrations of THNS and THAA were carbon-normalized. The decatal $SUVA_{254}$, the slope of absorbance at 275-295 nm ($Slope_{275-295}$), slope ratio of $Slope_{(275-295)}$ and $Slope_{(350-400)}$ (S_R), fluroescence index (FI), humification index (HIX), and the biological index (BIX) for all leachates.

Incubation	Sample	DOC (umol L^{-1})	THNS[a] (nmol mg C^{-1})	THAA[a] (nmol mg C^{-1})	Aromaticity[b] (umol OC L^{-1})	$SUVA_{254}$[c] (L mg C^{-1} m^{-1})	$S_{(275-295)}$[d]	S_R[e]	FI[f]	HIX[g]	BIX[h]
Grasses	t0	2018	2486	742	259	1.41	0.0102	0.56	1.40	0.51	0.75
	t1	1231	2220	271	206	2.01	0.0125	0.77	1.35	0.61	0.66
	t2	817	1693	536	175	2.73	0.0141	0.93	1.37	0.64	0.69
	t3	839	1669	400	150	2.18	0.0157	1.03	1.38	0.71	0.72
	t4	618	1343	477	115	2.29	0.0169	1.06	1.51	0.67	0.87
	t5	380	3748	637	95	3.29	0.0188	1.11	1.62	0.55	1.34
Cattails	t0	1242	1263	424	230	2.29	0.0125	0.70	1.41	0.68	0.56
	t1	955	1026	262	200	2.66	0.0143	0.89	1.23	0.68	0.57
	t2	799	973	283	178	2.86	0.0165	1.07	1.28	0.67	0.60
	t3	716	959	244	163	2.94	0.0168	1.08	1.29	0.64	0.64
	t4	628	983	239	132	2.66	0.0172	1.09	1.41	0.69	0.71
	t5	562	1122	305	115	2.59	0.0175	1.09	1.36	0.69	0.71
Pine	t0	4868	2398	122	472	0.93	0.0288	1.88	2.13	0.24	0.50
	t1	3917	1113	90	425	1.11	0.0291	1.84	1.75	0.24	0.51
	t2	3886	637	117	412	1.07	0.0318	2.01	1.79	0.26	0.50
	t3	1771	1107	158	255	1.65	0.0262	1.58	1.78	0.45	0.67
	t4	1897	1195	223	263	1.57	0.0265	1.63	1.72	0.48	0.49
	t5	1096	1226	95	195	2.17	0.0126	1.13	1.65	0.51	0.97
Tule	t0	1240	2243	241	203	1.95	0.0038	0.16	1.50	0.69	0.56
	t1	900	1899	194	174	2.40	0.0094	0.52	1.34	0.65	0.60
	t2	757	1629	135	162	2.72	0.0109	0.71	1.38	0.66	0.60
	t3	555	1067	190	136	3.20	0.0112	0.68	1.50	0.73	0.70
	t4	300	203	103	82	3.64	0.0142	0.90	1.53	0.88	0.69
	t5	314	197	123	89	3.80	0.0136	0.91	1.59	0.87	0.69
Oak	t0	9606	1825	139	2074	2.75	0.0225	1.11	2.17	0.68	0.23
	t1	5720	1570	62	1862	4.43	0.0214	1.30	2.01	0.66	0.29
	t2	5489	1210	48	1411	3.39	0.0136	1.24	1.72	0.78	0.29
	t3	3059	1016	56	1049	4.70	0.0124	1.03	1.60	0.91	0.31
	t4	3162	1004	61	1093	4.74	0.0129	1.05	1.67	0.91	0.31

Table 4 Continued.

[a] THNS and THAA concentrations (nmol L^{-1}) weighted to DOC (nmol L^{-1})

[b] % Aromaticity (% Aromaticity = 6.52($SUVA_{254}$) + 3.63) weighted to DOC (µmol L^{-1})

[c] $SUVA_{254}$ was calculated using the equation: $SUVA_{254} = \frac{a_{254}}{(2.303)(DOC)}$ where a_{254} is the absorption coefficent in m^{-1} and DOC is in mg L^{-1}

[d] Slope of the absorbance from 275-290 nm (Helms et al., 2008)

[e] Slope ratio (S_R) was determined using the ratio of the slope of 275-295 nm and slope 350-400 nm (Helms et al., 2008).

[f] Fluroescence index (FI) was determined using the ratio of emission wavelengths at 470 nm and 520 nm at excitation 370 nm (Cory and McKnight, 2005)

[g] Humification index (HIX) was calculated using the ratio of emission from area 435-480 nm and the combined area from 300-345 nm and 435-480 nm at excitation 254nm (Ohno, 2002).

[h] The biological/autochthonous index (BIX) was calculated using the ratio of emission at 380 nm and 430 nm at excitation 310 nm (Huguet et al., 2009)

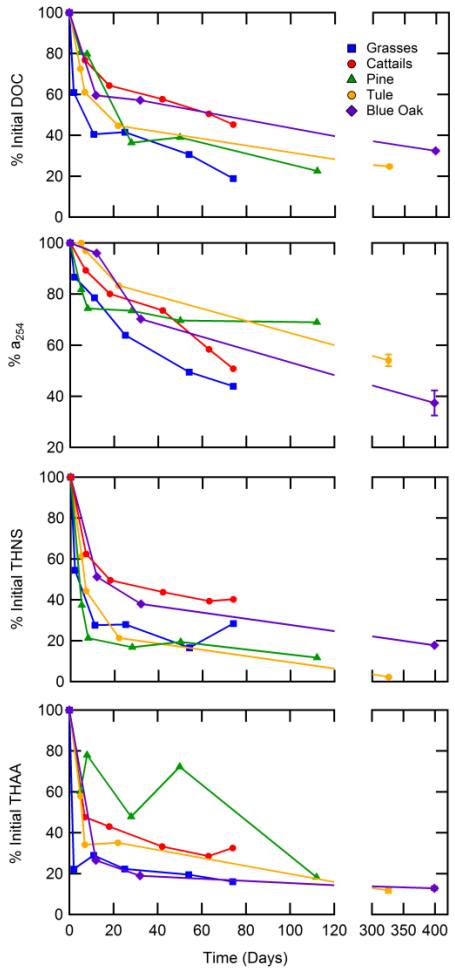

Figure 5 Percentage of initial DOC, absorption coefficient at 254 (a_{254}), initial THNS (%), and initial THAA (%) over time for time points in all coupled incubations. Initial percent change of DOC, a_{254}, THNS, and THAA were calculated by comparing time points' concentrations with initial concentrations.

THAA carbon-normalized concentrations ranged from 122 to 742 nmol mg C^{-1} in initial vascular plant leachates and 61 to 637 nmol mg C^{-1} at the end of the incubation experiments (Table 4). Initial carbon-normalized concentrations of THNS in vascular plant leachates ranged from 1263 to 2486 nmol mg C^{-1} and final carbon-normalized THNS concentrations after incubation experiments were 1004 to 3748 nmol mg C^{-1} (Table 4). Grasses leachate had higher carbon-normalized concentrations of THAA and

THNS than all other leachates. Carbon normalized concentrations of THNS decreased the most in tule leachate. In oak leachate, carbon normalized concentrations of THAA were lowest throughout all incubation experiments.

A 2-pool model was used to determine decay rate constants for the five vascular plant leachates to account for OC pools. Decay rate constants with standard deviations for DOC, THNS, and aromaticity are contained in Table 5. The decay rate constants of DOC, THNS, and aromaticity for all leachates best fit a single exponential model in these incubation experiments. DOC decay rate constants ranged from 0.052 to 0.411 day^{-1}, THNS decay rate constants ranged from 0.065 to 0.463 day^{-1}, and aromaticity decay rate constants ranged from 0.014 to 0.049 day^{-1} (Table 5). The decay rate constants were highest in THNS and lowest for aromaticity for all leachates. Grasses had the highest decay rate constants for DOC, THNS, and aromaticity. Oak had the lowest rate of decay for DOC and THNS, while cattails had the lowest rate of decay for aromaticity.

Table 5 Decay rate constants with standard deviation of DOC, THNS, and aromaticity in incubation samples.

Incubation	k_{DOC}	k_{THNS} (day^{-1})	$k_{Aromaticity}$
Grasses	0.411 ± 0.202	0.463 ± 0.107	0.049 ± 0.023
Cattails	0.068 ± 0.019	0.134 ± 0.018	0.014 ± 0.014
Pine	0.052 ± 0.016	0.289 ± 0.038	0.043 ± 0.014
Tule	0.086 ± 0.024	0.108 ± 0.023	0.043 ± 0.010
Oak	0.052 ± 0.037	0.065 ± 0.026	0.030 ± 0.008

[a] Single, single-stage exponential decay model using the following equation: $fit = y + a^{(-kx)}$
[b] k_{DOC} is the DOC decay rate constant
[c] k_{THNS} is the THNS decay rate constant
[d] $k_{Aromaticity}$ is the aromatic decay rate constant

Comparison of absorption coefficent at 254nm (a_{254}) of all time points to the initial (%) revealed a decrease in a_{254} during coupled incubations for all leachate types (Figure 5). Initial amounts of $SUVA_{254}$ had wide variation between leachates from 0.93 to 2.75 L mgC^{-1} m^{-1} (Table 4). Final $SUVA_{254}$ values ranged from 2.17 to 4.74 L mgC^{-1}

m^{-1} (Table 4). $SUVA_{254}$ increased with dose for all leachate types (Figure 6, Table 4). The spectral slope from the linear regression of absorbance at 275-295 nm ($S_{275-295}$) increased initially in grasses, cattails, and tule before plateauing with increasing dose, but decreased in pine and oak (Table 4, Figure 6). The ratio of the $S_{275-295}$ and the $S_{350-400}$ (S_R) increased with dose in grasses, cattails, and tule coupled incubations, but decreased in pine and oak (Table 4, Figure 6).

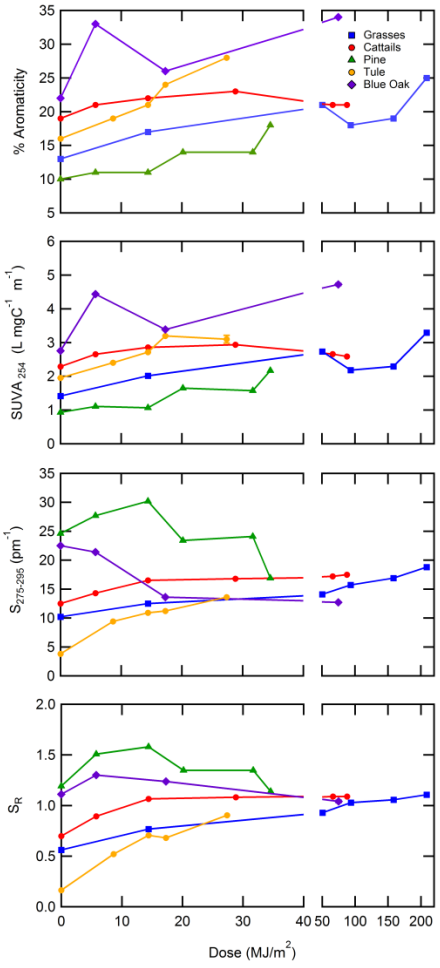

Figure 6 Aromaticity, $SUVA_{254}$, $slope_{(275-295)}$, and the slope ratio (S_R) for time points in all coupled incubations with increasing dose.

THNS yields indicate initial decomposition occurs in the neutral sugars quickly before plateauing in oak and pine (Figure 4). Tule continues to decrease throughout the incubation, and THNS yields for cattails change very little during the incubation. Grasses experiences a sharp rise at the end of the incubation (Figure 5). This large increase in THNS (% OC) might be attributed to continued degradation of DOC while the decomposition of the sugars decreased significantly. THAA yields changed gradually during the incubations for all leachates except grasses. Amino acids in grasses were quickly removed initially and experienced very little degradation after the initial removal, possibly due to the refractory pool of DOM.

The initial range of carbon-normalized THNS yields were 8 to 17 % OC (Figure 7, Table 7). Carbon normalized THAA yields ranged from 0.6 to 4.1 % OC in initial leachates (Figure 7, Table 6). THNS yields decreased during the incubation experiments with the exception of cattails, which had a relatively consistent yield of THNS with time, and grasses' THNS yield increased at the end of the incubation experiment (Figure 7). THAA yields (% OC) decreased from the initial for all leachate types. Grasses had the highest THAA yield of all leachate types while oak had the lowest. THNS yields were higher than THAA yields in vascular plant leachate.

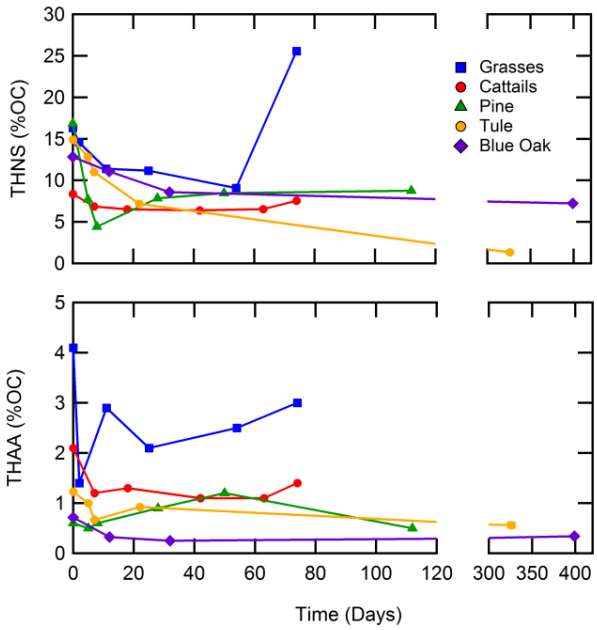

Figure 7 THNS carbon-normalized yields and THAA carbon-normalized yields for coupled incubations over time.

Changes in amino acid and neutral sugar composition are shown in Tables 6 and 7 and Figure 5. Asp and Gly (mol %) increase over the course of the incubation in all leachate types except oak, which had a decrease of Asp over time (Table 6).

The most abundant THAA in all leachates were Asx, Glx, Ser, Gly, and Ala (Table 6). Though the initial molar abundance of Glx ranged from 14-34 mol %, all five leachates had a molar abundance of 10-12 mol % of Glx at the end of the incubations (Table 7). Oak's initial Asp (mol %) was twice as abundant than in any other leachate during the course of the incubations but quickly decreased to the range of Asp in the other leachates (~10-20 mol %) (Table 7). After extensive degradation, tule displayed a rise in Gly and Phe abundance (Table 7). Oak had the largest shift in amino acid composition over the course of the incubation while cattails composition changed very little during the incubation (Table 7).

Table 6 THAA concentrations, THAA carbon-normalized yields, and relative abundance of THAA (mol %) composition of leachates.

Incubation	Sample	THAA ($\mu mol\ L^{-1}$)	THAA Yield (% OC)	D-AA (mol %)	Asp	Glu	Ser	His	Thr	Gly	Arg	Ala	Tyr	Val	Ile	Phe	Leu	Lys
					(mol %)													
Grasses	t0	18.0	4.1	5.4	10	18	6	2	9	11	3	13	2	8	3	5	7	5
	t1	4.0	1.4	4.0	15	14	10	1	8	18	2	12	1	7	4	4	5	2
	t2	5.3	2.9	5.3	13	12	8	1	7	15	3	12	2	6	3	6	6	5
	t3	4.0	2.1	7.8	14	12	9	1	7	16	3	13	1	6	3	7	5	4
	t4	3.5	2.5	8.7	14	11	9	1	7	17	3	13	1	6	2	7	5	4
	t5	2.9	3.0	11.0	15	12	9	1	8	18	3	16	1	6	2	0	5	4
Cattails	t0	6.3	2.1	2.4	15	14	10	1	7	19	2	12	1	6	2	3	5	3
	t1	3.0	1.2	4.4	16	12	11	1	7	23	1	12	1	5	2	3	4	2
	t2	2.7	1.3	4.6	16	11	10	1	7	23	1	13	1	5	2	3	4	2
	t3	2.1	1.1	5.6	17	11	10	0	7	23	2	13	1	5	3	2	4	2
	t4	1.8	1.1	7.2	16	11	10	0	7	25	1	14	0	5	2	2	3	2
	t5	2.1	1.4	6.8	17	11	9	0	7	24	2	14	0	5	2	2	4	3
Pine	t0	6.0	0.6	8.7	15	34	5	2	4	8	NA	18	1	4	2	3	3	2
	t1	3.6	0.5	19.9	21	19	6	2	4	13	NA	12	1	6	4	5	4	4
	t2	4.6	0.6	20.5	21	20	6	1	4	13	NA	12	2	6	3	4	4	4
	t3	2.8	0.9	10.9	17	17	7	1	5	13	NA	11	3	6	6	5	5	3
	t4	4.3	1.2	9.7	16	19	7	2	5	13	NA	12	3	7	4	5	6	3
	t5	1.1	0.5	14.4	19	12	8	1	5	18	NA	18	1	5	8	3	0	2
Tule	t0	3.6	1.2	6.7	18	17	9	1	7	16	2	11	2	5	3	4	4	2
	t1	2.1	1.0	6.8	16	16	10	1	6	16	3	11	2	5	3	4	5	2
	t2	1.2	0.7	13.8	18	11	8	0	7	19	1	14	2	6	4	4	4	2
	t3	1.3	0.9	12.7	20	13	9	1	8	18	2	13	1	6	2	3	3	1
	t4	0.4	0.5	14.3	13	9	5	0	6	32	2	12	1	3	1	12	2	2
	t5	0.5	0.6	11.9	13	10	6	1	5	30	2	12	1	3	1	12	3	2

Table 6 Continued.

Incubation	Sample	THAA ($\mu mol\ L^{-1}$)	THAA Yield (% OC)	D-AA (mol %)	Asp	Glu	Ser	His	Thr	Gly	Arg	Ala	Tyr	Val	Ile	Phe	Leu	Lys
					(mol %)													
Oak	t0	16.0	0.7	6.4	41	15	5	3	3	11	2	7	2	4	2	2	2	2
	t1	4.3	0.3	8.8	18	13	9	2	6	17	2	10	3	5	5	4	4	3
	t2	3.2	0.3	10.5	18	12	9	1	6	17	2	11	3	6	5	4	5	3
	t3	2.0	0.3	3.4	11	11	6	0	5	10	3	12	2	8	6	7	17	3
	t4	2.3	0.4	4.1	12	11	5	0	5	11	3	11	2	8	5	7	17	3

NA, not available.

Table 7 THNS concentrations, THNS carbon-normalized yields, and relative abundance of THNS (mol %) composition of leachates.

Incubation	Sample	THNS ($\mu mol\ L^{-1}$)	THNS Yield (% OC)	Fuc	Rha	Ara	Gal	Glc	Man	Xyl
				(mol %)						
Grasses	t0	60	16	1	4	14	12	26	4	39
	t1	33	15	3	7	16	15	17	5	37
	t2	17	11	6	12	15	17	20	6	24
	t3	17	11	6	13	16	16	17	6	26
	t4	10	9	8	15	13	12	20	8	24
	t5	17	26	8	15	11	16	19	10	21
Cattails	t0	19	8	1	4	17	16	27	3	31
	t1	12	7	2	4	19	21	25	3	25
	t2	9	7	5	7	15	14	27	7	27
	t3	8	6	4	6	16	14	25	7	29
	t4	7	7	7	7	20	15	20	3	27
	t5	8	8	10	8	15	15	23	4	25
Pine	t0	119	17	1	7	9	5	69	5	5
	t1	44	8	2	19	14	10	39	7	10
	t2	25	4	3	25	17	12	32	6	6
	t3	20	8	5	28	6	25	26	6	3
	t4	23	8	4	25	6	31	23	6	5
	t5	14	9	9	14	2	40	24	8	3
Tule	t0	33	15	1	3	19	15	30	4	28
	t1	20	13	2	6	20	24	26	5	17
	t2	15	11	2	5	18	21	26	7	20
	t3	7	7	6	6	14	13	33	3	25
	t4	1	1	6	6	16	9	29	6	28
	t5	1	1	4	5	16	8	33	4	29
Oak	t0	210	13	1	18	8	9	54	3	6
	t1	108	11	1	36	7	16	33	2	6
	t2	80	9	16	53	13	42	47	7	9
	t3	37	7	22	10	2	18	35	11	3
	t4	38	7	21	11	2	17	36	12	2

In all leachate incubations, THNS molar abundance of Fuc (mol %) increased over time (Table 7). Rha (mol%) increased in grasses and pine and increased during the beginning of the oak incubation before decreasing again in the final time points of oak (Table 7). Gal (mol %) increased in pine and oak time points as well as a small increase in grasses time points over the incubation period (Table 7). Glc abundance was high in all leachates and decreased in all incubations except tule (Table 7). The pine and oak leachates had the largest change in Glc abundance (25% and 18% change respectively) (Table 7). Man increased in grasses and oak time points, and Xyl decreased in grasses and cattails (Table 7).

A principal component analysis (PCA) on THNS composition and THAA composition revealed distinctions between the compositions in leachates during coupled incubations (Figure 8). Pine leachate THAA compositions were dominated by Asx, Glx, and His throughout the incubation with increasing abundance of Gly and Tyr. THAA composition in oak leachate was dominated by Asx, Glx, and His. Over the course of the incubation, oak leachates were enriched in Leu and Val. Tule THAA abundance was driven by changes in Gly and Asx. Cattails THAA abundance had minor changes of abundance in Gly during the incubation.

The principal component analysis of THNS molar abundance revealed an enrichment of Xyl and Ara in grasses, cattails, and tule, while oak and pine initially were enriched in Glc and Rha with a shift to Gal, Man, and Fuc over the time of the incubation (Figure 8). Oak and pine THNS composition were distinctly different to neutral sugar abundance in grasses, cattails, and tule leachates throughout coupled incubations (Figure 8). Glc and Rha abundance led initial THNS molar abundances in oak and pine leachates significantly (Figure 8). As Glc abundance decreased, Gal abundance increased in oak and pine. THNS abundance shifted towards Gal, Fuc, and Man in oak. Xyl and Ara abundance (mol %) for tule leachate were most significant, and there was a shift from Gal to Glc abundance over time.

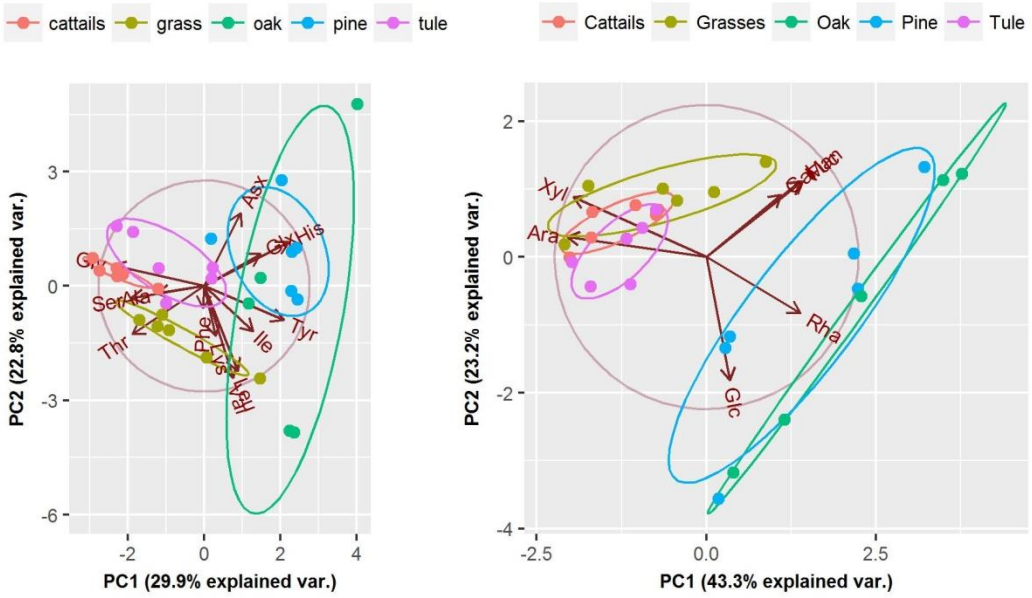

Figure 8 Principal component analyses (PCA) of relative abundance of THAA and relative abundance of THNS for all coupled incubation time points. A 95% confidence ellipsis was applied to describe the region where 95% of the time a point would be estimated.

All leachate types demonstrated an increase in D-AA concentrations (nmol mg C^{-1}) during the coupled incubations except oak which had decreasing D-AA concentrations during the incubation (Figure 9). The molar abundance of D-AA (mol %) increased in all leachates with the exception of a decrease in oak D-AA in the last time point (Table 6, Figure 9). The relative abundance of glycine (mol %) increased in all coupled incubations, but the glycine in oak leachate decreased in the final time point (Table 6, Figure 9).

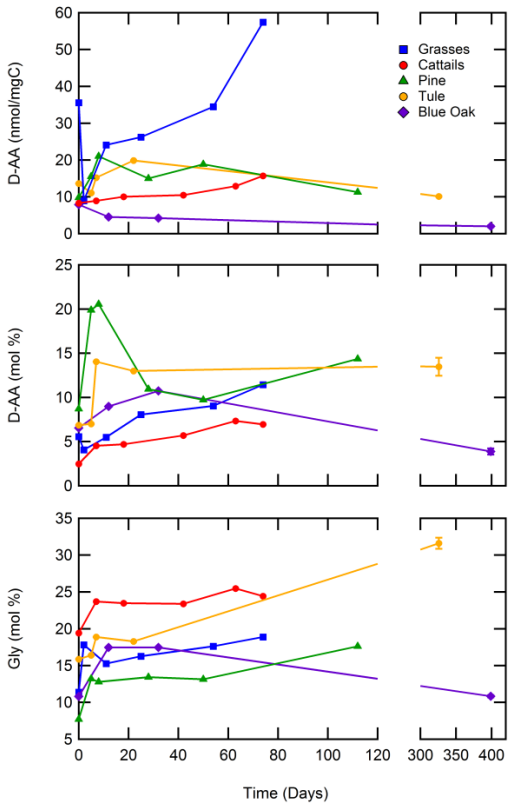

Figure 9 Concentration of D-AA, relative abundance of D-AA, and relative abundance of Gly (mol %) over time for all coupled incubations.

3.3 Salinity Relationships with Biomarkers, Optical Proxies, and Biolabile DOC

Three transects were sampled in the San Joaquin/ Sacramento River Delta through the San Francisco Bay Estuary. A winter transect at maximum winter discharge was collected to study the DOM dynamics largely in the absence of photodegradation processes and low levels of algal production, while two summer transects were taken during significant photodegradation and algal production conditions. The 2014 transect was collected during December, the 2015 transect was collected during June, and the 2016 transect was collected during May. In addition to transect samples, samples at four sampling sites were collected representing river and marine endmembers: Vernalis (San Joaquin river end), Garcia Bend (Sacramento River end), Belden's Landing, and the Golden Gate Bridge (marine end). The rest of the chosen stations in each transect were

decided based on the salinity at the site with higher density sampling at low salinities taken across an axial transect from river to coastal ocean (Figure 4).

California's Department of Water Resources employs a model to estimate discharge in the Sacramento-San Joaquin River Delta to the San Francisco Bay known as Dayflow. The estimates calculated by Dayflow have been used during collection of the three transects to compare hydrologic conditions and are summarized in Table 8 by the day of collection and the total discharge (m^3s^{-1}) for the month of collection. December 2014 discharge totaled at 957 m^3s^{-1} from the Sacramento River upstream of the Delta, 35 m^3s^{-1} from the San Joaquin River to the Delta, and Dayflow estimated a net Delta outflow of 969 m^3s^{-1} to the Bay for the month. Fresh rainfall the night before sampling caused flushing conditions with high discharge river flow during December 2014 collection. Collection of the 2014 transect occurred on December 20th. Discharge on the day of collection was measured at 718 m^3s^{-1} from the Sacramento River, 23 m^3s^{-1} from San Joaquin River, and 767 m^3s^{-1} outflow to the Bay (California Department of Water Resources, Dayflow, 2017).

June of 2015 outflow conditions from the Sacramento River totaled 192 m^3s^{-1} to the Delta, San Joaquin River totaled 5 m^3s^{-1} in the river, and Dayflow estimated a net Delta outflow of 106 m^3s^{-1} to the Bay for the month. Below average precipitation coupled with drought conditions during the 2015 transect caused river conditions during sampling to be low to no flow in areas with standing pools and algae blooms. Collection of the 2015 transect occurred on June 15th. Discharge on the day of collection was measured at 90 m^3s^{-1} from the Sacramento River, 2 m^3s^{-1} from San Joaquin river, and 37 m^3s^{-1} outflow to the Bay (California Department of Water Resources, Dayflow, 2017).

May of 2016 outflow conditions in the Sacramento River totaled 385 m^3s^{-1} upstream of the Delta, discharge from the San Joaquin River totaled 56 m^3s^{-1} flow in the river and a net Delta outflow of 351 m^3s^{-1} to the Bay. Low precipitation and higher phytoplankton production occurred in this summer collection compared to the winter collection (December 2014), but the transect in 2016 had higher riverine discharge than the transect in 2015. Discharge during collection on May 2nd, 2016 from the Sacramento

River was 150 m^3s^{-1}, the San Joaquin was 37 m^3s^{-1}, and estimated outflow from the Delta to the Bay was 134 m^3s^{-1} (California Department of Water Resources, Dayflow, 2017).

Table 8 Discharge (m^3s^{-1}) from the Sacramento River, San Joaquin River, and outflow from the Sacramento-San Joaquin River Delta to the San Francisco Bay on the day of collection for the 2014, 2015, and 2016 transects and during the entire month.

	Collection	Sacramento River	San Joaquin River (m^3s^{-1})	Delta
Day	20-Dec-14	718	23	767
	15-Jun-15	90	2	37
	2-May-16	150	37	134
Month	December 2014	957	35	969
	June 2015	192	5	106
	May 2016	385	56	351

Salinity in the Delta-Bay is affected by tidal-influence, precipitation, and freshwater discharge from upstream. In the winter transect taken in 2014, salinity in the river and upper Delta stations ranged from 0.1 to 0.5 psu (Figure 10, Table 9). Salinity increased in Suisun Bay and Belden's Landing before reaching 27.8 psu at the Golden Gate Bridge (Table 9). Salinity in the summer transect collected in 2015 ranged from 0.1 to 30.1 psu (Table 10). Salt water intrusion into the Delta was evident up to Sherman Island as seen in Figure 10. In 2016, salinity ranged from 0.1 to 28.3 psu, and salinity values began increasing from Chain Island with a salinity of 1.1 psu (Figure 10, Table 11). Salinity values were highest in the 2015 transect compared to the 2014 and 2016 transects (Figure 10).

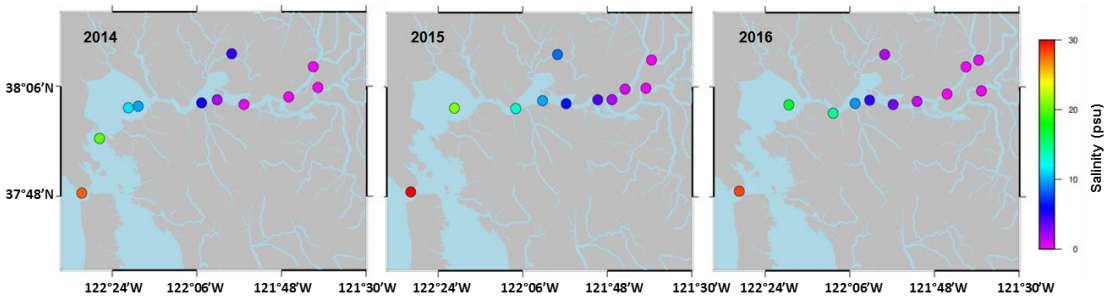

Figure 10 Measured salinities in the Sacramento-San Joaquin River Delta and San Francisco Bay during transect collection in 2014, 2015, and 2016.

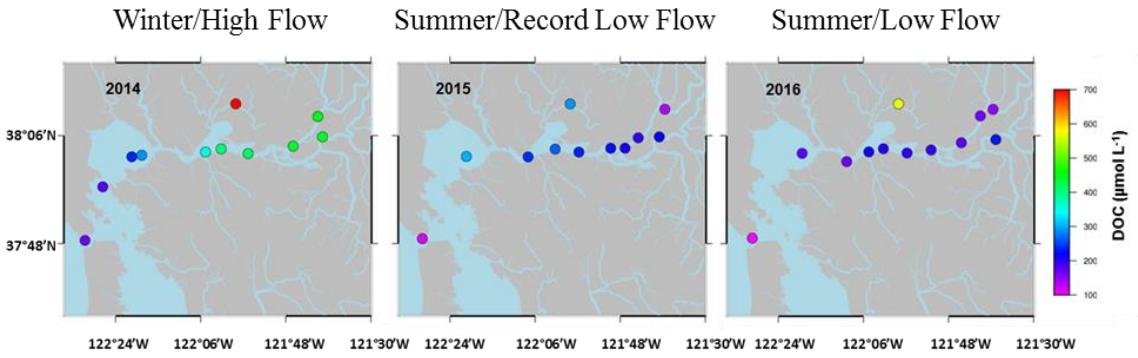

Figure 11 DOC concentrations in the Sacramento-San Joaquin River Delta and San Francisco Bay during transect collection in 2014, 2015, and 2016.

Table 9 Samples collected in the 2014 transect of the Sacramento River/San Joaquin River Delta and San Francisco Bay Estuary were analyzed for DOC concentrations, optical absorption, and fluorescence. Concentrations of THNS and THAA were carbon-normalized. The decatal $SUVA_{254}$, the slope of absorbance at 275-295 nm ($S_{275-295}$), slope ratio of $S_{(275-295)}$ and $S_{(350-400)}$ (S_R), fluroescence index (FI), humification index (HIX), and the biological index (BIX) for all stations.

Site Name	Lat	Long	Salinity (PSU)	DOC (umol L^{-1})	$TDLP_9$ [a] (nmol mgC^{-1})	THNS[b] (nmol mgC^{-1})	THAA[b] (nmol mgC^{-1})	Aromaticity[c] (umol OC L^{-1})	$SUVA_{254}$[d] (L mgC^{-1} m^{-1})	$S_{(275-295)}$[e]	S_R [f]	FI [g]	HIX [h]	BIX [i]
Golden Gate Bridge	37.8087	-122.5080	27.8	167	0.80	381	1291	10	0.3523	0.0283	NA*	1.64	0.72	0.78
San Rafael Bay	37.9575	-122.4451	20.2	178	1.33	460	356	18	1.0410	0.0187	0.96	1.62	0.76	0.76
San Pablo Bay	38.0413	-122.3430	11.4	239	1.46	393	541	26	1.1382	0.0177	0.78	1.59	0.81	0.74
San Pablo Bay (Entrance)	38.0455	-122.3078	9.9	288	1.51	397	453	32	1.1470	0.0167	0.77	1.62	0.84	0.70
Lower Susan Bay	38.0545	-122.0830	5.5	354	1.57	509	1058	41	1.2288	0.0157	0.79	1.61	0.86	0.68
Belden's Landing	38.1879	-121.9762	4.9	706	1.70	687	496	86	1.3131	0.0158	0.77	1.56	0.90	0.64
Roe Island	38.0629	-122.0279	1.9	403	1.62	577	941	51	1.3681	0.0149	0.80	1.60	0.88	0.64
Chipps Island	38.0502	-121.9329	0.4	413	1.65	510	504	54	1.4633	0.0148	0.75	1.58	0.89	0.61
Sherman Island	38.0706	-121.7742	0.1	436	1.65	534	932	54	1.3392	0.0144	0.74	1.61	0.89	0.63
Twitchell Island	38.0965	-121.6705	0.2	439	1.64	658	660	55	1.3620	0.0152	0.74	1.55	0.91	0.61
Rio Vista	38.1529	-121.6868	0.1	448	1.67	882	503	59	1.4524	0.0144	0.72	1.58	0.90	0.62
Vernalis	37.6793	-121.2650	0.5	645	1.70	815	652	76	1.2543	0.0153	0.76	1.65	0.88	0.70
Garcia Bend	38.4778	-121.5433	0.1	417	1.64	787	716	53	1.3736	0.0148	0.71	1.55	0.88	0.61

[a] $TDLP_9$, sum of *p*-hydroxy, vanillyl, and syringyl phenols

[b] THNS and THAA concentrations (nmol L^{-1}) weighted to DOC (nmol L^{-1})

[c] % Aromaticity (% Aromaticity = 6.52($SUVA_{254}$) + 3.63) weighted to DOC (µmol L^{-1})

[d] $SUVA_{254}$ was calculated using the equation: $SUVA_{254} = \frac{a_{254}}{(2.303)(DOC)}$ where a_{254} is the absorption coefficent in m^{-1} and DOC is in mg L^{-1}

[e] Slope of the absorbance from 275-290 nm (Helms et al., 2009)

[f] Slope ratio (S_R) was determined using the ratio of the slope of 275-295 nm and slope 350-400 nm (Helms et al., 2008).

[g] Fluroescence index (FI) was determined using the ratio of emission wavelengths at 470 nm and 520 nm at excitation 370 nm (Cory and McKnight, 2005)

[h] Humification index (HIX) was calculated using the ratio of emission from area 435-480 nm and the combined area from 300-345 nm and 435-480 nm at excitation 254nm (Ohno, 2002).

[i] The biological/autochthonous index (BIX) was calculated using the ratio of emission at 380 nm and 430 nm at excitation 310 nm (Huguet et al., 2009)

* Not Available

Table 10 Samples collected in the 2015 transect of the Sacramento River/San Joaquin River Delta and San Francisco Bay Estuary were analyzed for DOC concentrations, optical absorption, and fluorescence. Concentrations of THNS and THAA were carbon-normalized. The decatal $SUVA_{254}$, the slope of absorbance at 275-295 nm ($S_{275-295}$), slope ratio of $S_{(275-295)}$ and $S_{(350-400)}$ (S_R), fluroescence index (FI), humification index (HIX), and the biological index (BIX) for all stations.

Site Name	Lat	Long	Salinity (PSU)	DOC (umol L^{-1})	$TDLP_9$ [a] (nmol mgC^{-1})	THNS[b] (nmol mgC^{-1})	THAA[b] (nmol mgC^{-1})	Aromaticity[c] (umol OC L^{-1})	$SUVA_{254}$[d] (L mgC^{-1} m^{-1})	$S_{(275-295)}$[e]	S_R [f]	FI [g]	HIX [h]	BIX [i]
Golden Gate Bridge	37.8136	-122.4975	30.1	117	0.83	527	1518	9	0.6244	0.0229	0.80	1.63	0.76	0.90
San Pablo Bay	38.0422	-122.3423	21.2	304	1.32	218	176	25	0.7113	0.0192	1.09	1.57	0.79	0.83
Benicia	38.0410	-122.1250	13.3	241	1.39	386	219	27	1.1470	0.0189	0.98	1.55	0.85	0.80
Roe Island	38.0624	-122.0294	9.9	266	1.40	384	352	29	1.1233	0.0188	1.03	1.55	0.84	0.78
Belden's Landing	38.1879	-121.9762	8.6	291	1.52	508	1091	41	1.6256	0.0181	0.95	1.56	0.88	0.72
Honker Bay	38.0542	-121.9459	6.4	236	1.41	562	532	28	1.2686	0.0185	1.01	1.56	0.86	0.76
Chain Island	38.0649	-121.8335	4.1	228	1.39	437	1127	27	1.2476	0.0189	0.99	1.55	0.86	0.75
Sherman Island	38.0651	-121.7832	1.8	206	1.35	565	1448	23	1.1612	0.0191	0.99	1.53	0.85	0.75
Decker Island	38.0938	-121.7366	0.7	195	1.31	499	1036	21	1.1083	0.0193	0.96	1.54	0.85	0.74
Twitchell Island	38.0964	-121.6627	0.4	214	1.39	635	1021	26	1.2842	0.0185	1.01	1.53	0.85	0.73
Ida Island	38.1730	-121.6428	0.1	135	1.16	1099	1523	14	1.0560	0.0207	0.93	1.61	0.79	0.79
Vernalis	37.6375	-121.2013	0.3	167	1.34	1190	1194	20	1.2411	0.0179	0.97	1.67	0.84	0.77
Garcia Bend	38.4778	-121.5433	0.1	126	1.16	1054	2771	14	1.1295	0.0203	0.98	1.55	0.79	0.74

[a] $TDLP_9$, sum of *p*-hydroxy, vanillyl, and syringyl phenols

[b] THNS and THAA concentrations (nmol L^{-1}) weighted to DOC (nmol L^{-1})

[c] % Aromaticity (% Aromaticity = $6.52(SUVA_{254}) + 3.63$) weighted to DOC (µmol L^{-1})

[d] $SUVA_{254}$ was calculated using the equation: $SUVA_{254} = \frac{a_{254}}{(2.303)(DOC)}$ where a_{254} is the absorption coefficent in m^{-1} and DOC is in mg L^{-1}

[e] Slope of the absorbance from 275-290 nm (Helms et al., 2009)

[f] Slope ratio (S_R) was determined using the ratio of the slope of 275-295 nm and slope 350-400 nm (Helms et al., 2008).

[g] Fluroescence index (FI) was determined using the ratio of emission wavelengths at 470 nm and 520 nm at excitation 370 nm (Cory and McKnight, 2005)

[h] Humification index (HIX) was calculated using the ratio of emission from area 435-480 nm and the combined area from 300-345 nm and 435-480 nm at excitation 254nm (Ohno, 2002).

[i] The biological/autochthonous index (BIX) was calculated using the ratio of emission at 380 nm and 430 nm at excitation 310 nm (Huguet et al., 2009)

Table 11 Samples collected in the 2016 transect of the Sacramento River/San Joaquin River Delta and San Francisco Bay Estuary were analyzed for DOC concentrations, optical absorption, and fluorescence. Concentrations of THNS and THAA were carbon-normalized. The decatal $SUVA_{254}$, the slope of absorbance at 275-295 nm ($S_{275-295}$), slope ratio of $S_{(275-295)}$ and $S_{(350-400)}$ (S_R), fluroescence index (FI), humification index (HIX), and the biological index (BIX) for all stations.

Site Name	Lat	Long	Salinity (PSU)	DOC (umol L^{-1})	$TDLP_9$ [a] (nmol mgC^{-1})	THNS[b] (nmol mgC^{-1})	THAA[b] (nmol mgC^{-1})	Aromaticity[c] (umol OC L^{-1})	$SUVA_{254}$[d] (L mgC^{-1} m^{-1})	$S_{(275-295)}$[e]	S_R [f]	FI [g]	HIX [h]	BIX [i]
Golden Gate Bridge	37.8155	-122.49224	28.3	98	1.42	430	274	13	1.4539	0.0174	0.99	1.56	0.85	0.72
San Pablo Bay	38.0509	-122.31624	16.8	175	1.43	661	546	22	1.3956	0.0174	0.90	1.54	0.87	0.70
Benicia	38.0281	-122.15902	14.4	167	1.38	377	361	23	1.5393	0.0169	1.05	1.56	0.71	0.77
Lower Susan Bay	38.0549	-122.08100	9.6	209	1.39	366	633	38	2.2051	0.0183	0.63	1.56	0.49	0.75
Roe Island	38.0638	-122.02977	4.7	202	1.28	506	169	25	1.3438	0.0190	1.02	1.57	0.76	0.74
Honker Bay	38.0519	-121.94631	3.2	197	1.33	583	436	26	1.4653	0.0186	0.94	1.55	0.73	0.73
Belden's Landing	38.1879	-121.97627	1.6	567	1.41	499	377	70	1.3401	0.0179	0.95	1.54	0.84	0.73
Chain Island	38.0603	-121.86140	1.1	194	1.42	761	493	21	1.1284	0.0176	0.86	1.56	0.85	0.69
Decker Island	38.0803	-121.75498	0.1	177	1.26	754	1674	31	2.1216	0.0187	0.76	1.55	0.50	0.74
Twitchell Island	38.0890	-121.63325	0.1	232	1.64	631	415	31	1.4851	0.0170	0.87	1.55	0.87	0.65
Ida Island	38.1727	-121.64324	0.1	149	0.68	753	455	25	2.0029	0.0225	0.56	1.75	0.19	1.18
Rio Vista	38.1545	-121.68765	0.1	166	1.32	750	1360	19	1.1969	0.0183	1.08	1.54	0.79	0.77
Vernalis	37.6793	-121.26506	0.1	249	1.34	525	371	33	1.4671	0.0182	1.00	1.55	0.71	0.80
Garcia Bend	38.4778	-121.54336	0.1	127	1.36	629	690	16	1.3232	0.0178	0.78	1.53	0.69	0.78

[a] $TDLP_9$, sum of *p*-hydroxy, vanillyl, and syringyl phenols

[b] THNS and THAA concentrations (nmol L^{-1}) weighted to DOC (nmol L^{-1})

[c] % Aromaticity (% Aromaticity = 6.52($SUVA_{254}$) + 3.63) weighted to DOC (µmol L^{-1})

[d] $SUVA_{254}$ was calculated using the equation: $SUVA_{254} = \frac{a_{254}}{(2.303)(DOC)}$ where a_{254} is the absorption coefficent in m^{-1} and DOC is in mg L^{-1}

[e] Slope of the absorbance from 275-290 nm (Helms et al., 2009)

[f] Slope ratio (S_R) was determined using the ratio of the slope of 275-295 nm and slope 350-400 nm (Helms et al., 2008).

[g] Fluroescence index (FI) was determined using the ratio of emission wavelengths at 470 nm and 520 nm at excitation 370 nm (Cory and McKnight, 2005)

[h] Humification index (HIX) was calculated using the ratio of emission from area 435-480 nm and the combined area from 300-345 nm and 435-480 nm at excitation 254nm (Ohno, 2002)

[i] The biological/autochthonous index (BIX) was calculated using the ratio of emission at 380 nm and 430 nm at excitation 310 nm (Huguet et al., 2009)

In the 2014 transect, DOC concentrations ranged from 167 to 706 μmol L^{-1} decreased from the Delta to the Bay with the lowest concentration at the marine end, Golden Gate Bridge (Table 9). DOC concentrations in the 2015 transect were highest at San Pablo Bay (Station 2) and Belden's Landing (Table 10). Golden Gate Bridge had the lowest DOC concentration (117 μmol L^{-1}), and Vernalis and Garcia Bend DOC concentrations were ~150 (nmol mg C^{-1}) while Bay stations (stations 2-6) had concentrations greater than 200 (nmol mg C^{-1}). In the 2016 transect samples, DOC concentrations were highest at Belden's Landing followed by Vernalis and riverine stations, and the lowest DOC concentration was at Golden Gate Bridge (Table 11). DOC concentrations were highest in the 2014 transect compared to the 2015 and 2016 transects. Concentrations were greater in the Rivers and Delta in 2014 and greater in the Bay stations in 2015 and 2016 (Figure 11).

In 2014, carbon-normalized THNS concentrations ranged from 381 to 882 nmol mg C^{-1} and were highest in Vernalis and Garcia Bend and decreased through the Delta-Bay (Table 9). In 2015, carbon-normalized THNS concentrations ranged from ~200 to > 1000 nmol mg C^{-1} where River sites such as Vernalis and Garcia Bend had significantly high carbon-normalized concentrations (> 1000 nmol mg C^{-1}) of THNS and Bay sites had lower concentrations (Table 10). Carbon-normalized THNS concentrations ranged from 366 to 761 nmol mg C^{-1} in 2016 were higher at Delta sites compared to Bay sites (Table 11).

The highest carbon-normalized THAA concentration in the 2014 transect was at the Golden Gate Bridge, though stations 5, 6, and 8 had concentrations > 900 nmol mg C^{-1} (Table 9). Vernalis and Garcia Bend had ~800 nmol mg C^{-1}, and concentrations in the transect ranged from 356 to 1291 nmol mg C^{-1} (Table 9). In the 2015 transect, several sampled sites had high carbon-normalized concentrations of THAA, including the Golden Gate Bridge, Belden's Landing, Delta stations, and the two river ends Vernalis and Garcia Bend and carbon-normalized concentrations of THAA ranged from 176 to 2771 nmol mg C^{-1} (Table 10). THAA carbon-normalized concentrations for 2016 were elevated (~2000 nmol mg C^{-1}) in two Delta stations, at stations 9 and 12 in the

2016 transect while other low salinity (0.1 ppt) sites had carbon-normalized concentrations of about 450 to 840 nmol mg C^{-1} and the Golden Gate Bridge had a THAA carbon-normalized concentration of 395 nmol mg C^{-1} (Table 11).

Aromaticity concentrations in the 2014 transect ranged from 10 to 86 nmol mg C^{-1} and decreased along the transect gradient with a notable exception at the sample site Belden's Landing, which had the highest concentration of aromatic carbons (Table 9). Aromaticity concentrations ranged from 9 to 41 nmol mg C^{-1} in the 2015 transect were highest at Belden's Landing and at stations in the middle of the transect, or lower Delta, and the lowest was at Golden Gate Bridge (Table 10). Carbon-normalized aromaticity concentrations in the 2016 transect ranged from 13 to 71 nmol mg C^{-1} and were highest in Belden's Landing and lowest at Golden Gate Bridge and Garcia Bend (Table 11). Aromaticity yields in the 2014 transect were highest in the Delta, lower in the Bay, and depleted in the marine endmember (Figure 12). Aromaticity yields in the 2015 transect were similar in the Delta and upper Bay, depleted in the Bay and marine endmember, and enriched at Belden's Landing (Figure 12). The 2016 transect had the highest aromaticity yields and demonstrated variability throughout the Delta, Bay, and marine endmember (Figure 12).

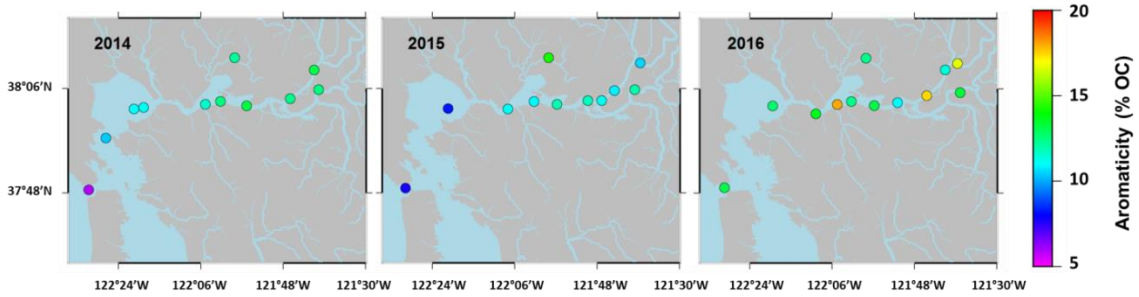

Figure 12 Aromaticity yields (% OC) in the 2014, 2015, and 2016 transects.

$SUVA_{254}$ was higher in the Delta than in the Bay in the 2014 transect while S_R and $S_{(275-295)}$ decreased from the Delta to the Bay (Table 9). $SUVA_{254}$ in 2015 ranged

from 0.6244 to 1.6256 L mg C^{-1} m^{-1} and decreased from the Delta to the Bay in the 2015 transect except at Belden's Landing, which had the highest $SUVA_{254}$ value (Table 10). S_R ranged from 0.93-1.09 in the rivers, Delta and Bay sites in 2015, but Golden Gate Bridge had a lower value at 0.80. $S_{(275-295)}$ was highest in the Golden Gate Bridge followed by the Garcia Bend and Station 9. The rest of the 2015 transect sites demonstrated an increase in $S_{(275-295)}$ moving through the Delta to the Bay. In 2016, $SUVA_{254}$ ranged from 1.1284 to 2.2051 L mg C^{-1} m^{-1}. There were no apparent trends for $SUVA_{254}$ with salinity or location in the transect. Stations 8 and 12 had the lowest $SUVA_{254}$ values in the 2016 transect, and the highest values were at stations 4, 9 and 11 (Table 11). $SUVA_{254}$ values at Golden Gate Bridge, Garcia Bend, and Vernalis were relatively uniform. S_R values were between 0.63 and 1.08 in the 2016 transect. $S_{(275-295)}$ ranged 0.0169 to 0.0225 L mg C^{-1} m^{-1} and was elevated in station 11 (Ida Island) compared to other 2016 stations, and values of $S_{(275-295)}$ were lower in the Bay stations than in the Delta (Table 11).

The FI ranged from 1.53 to 1.67 in all transect samples except station 10 (Ida Island) in the 2016 transect, which had a significantly high FI value of 1.75 (Table 9, 10, 11). FI values were lowest in the 2016 transect (with the exception of the outlying value at station 10), but FI values were within similar ranges in all three transects and did not display clear trends with salinity. HIX normalized values ranged from 0.72 to 0.91 and displayed a general decrease from the Delta to the Bay. HIX in 2015 varied from 0.76 to 0.88 and was lowest in the marine endmember (Table 10). Normalized HIX values ranged in the 2016 transect from 0.49 to 0.87 with station 11 (Ida Island) had an outlying value of 1.18 (Table 11). Normalized HIX values were lower in 2016 (with the exception of station 11) than in 2014 and 2015. HIX values had a similar ranged in 2014 and 2015. While in the 2014 and 2015 transects, HIX values were higher in the Delta than the Bay, the 2016 HIX values varied throughout the transect with low values measured in the Delta. 2014 BIX values (0.61 to 0.78) were highest in the Delta and lowest in the marine end (Table 9). BIX was highest in the marine end (Golden Gate Bridge, 0.9) and ranged from 0.72 to 0.83 in the rest of the 2015 transect. BIX values

were lower in the river and Delta stations than in the Bay stations (Table 10). BIX values throughout the 2016 transect varied from 0.65-0.80 at most stations, and station 11 had an outlying BIX value of 1.18 (Table 11). The 2015 transect had the lowest BIX range (excluding station 11 in the 2016 transect). BIX values were generally higher in 2014 than the other transects.

Tables 12-14 contain the THNS concentrations (μmol L^{-1}), THNS carbon-normalized yields, and molar abundance of neutral sugars for the 2014, 2015, and 2016 transects. THNS concentrations (μmol L^{-1}) decreased with increasing salinity in 2014 stations (Table 12). THNS carbon-normalized yields (% OC) were highest in Delta sites and lower within the Bay, ranging from ~2.7-6.1 % OC (Figure 13). Golden Gate had the lowest carbon-normalized yield of THNS (2.65 % OC). Glc had the highest abundance of all neutral sugars in 2014 stations (18-39 mol %) (Table 12). Rha, Ara, Gal, and Man were elevated in Vernalis and Garcia Bend compared to Golden Gate while Glc was elevated in Golden Gate. Fuc increased in abundance in the 2014 transect with increasing salinity except in the marine end (Golden Gate). Man decreased in abundance with increasing salinity (Table 12). The 2015 transect had THNS concentrations from ~0.7 μmol L^{-1} in Bay stations to >1.5 μmol L^{-1} in Delta stations (Table 13). THNS carbon-normalized yields were between 1.5-8.3 % OC and decreased into the Bay (Figure 13). Carbon-normalized THNS yields at Vernalis and Garcia Bend were twice as high as Golden Gate and Belden's Landing (Table 13). 2015 stations had a high abundance of Glc (14-24 mol %), and Golden Gate had the lowest abundance of Glc and the highest abundance of Gal. Fuc abundance was 15-23 mol% in 2015 stations (Table 13). Rha abundance was uniform across the 2015 transect. Ara was abundant in Bay sites, and Man was abundant in Delta stations (Table 13). THNS concentrations were highest at Belden's Landing for the 2016 stations, and except for Belden's Landing and Garcia Bend, THNS concentrations decreased with increasing salinity (Table 14). THNS carbon-normalized yields in 2016 were between ~2.5-5.2 % OC. Glc was the most abundant sugar in lower salinity stations and station 2. Fuc was highest at Golden

Gate compared to the rest of the 2016 transect, and the most abundant sugar at Golden Gate.

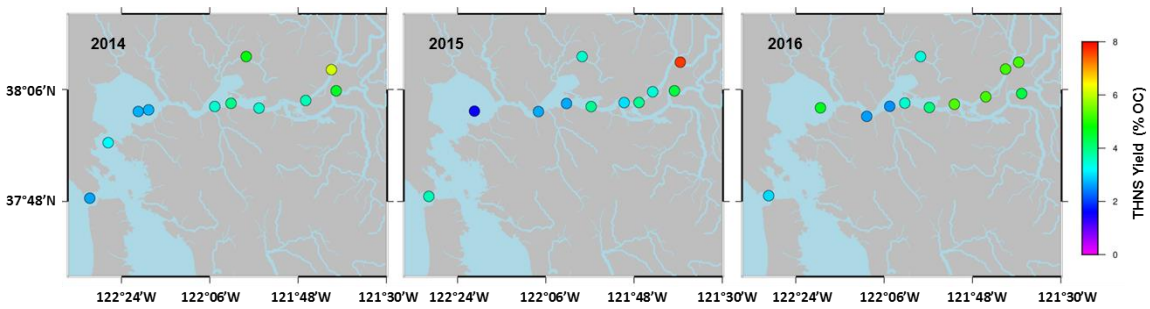

Figure 13 Carbon-normalized THNS yields (% OC) in the 2014, 2015, and 2016 transects.

Table 12 2014 transect THNS concentrations, THNS carbon-normalized yields, and molar percentage of THNS (mol %).

Site Name	THNS ($\mu mol\ L^{-1}$)	THNS Yield (% OC)	Fuc	Rha	Ara	Gal	Glc	Man	Xyl
			(mol %)						
Golden Gate Bridge	0.76	2.64	12	8	9	10	39	6	15
San Rafael Bay	0.98	3.18	13	14	11	16	21	12	13
San Pablo Bay	1.12	2.71	16	16	11	14	23	6	13
San Pablo Bay (Entrance)	1.37	2.73	17	18	12	14	20	6	14
Lower Susan Bay	2.16	3.49	17	15	11	13	20	7	17
Belden's Landing	5.83	4.74	15	13	12	18	18	11	14
Roe Island	2.79	3.97	16	16	11	14	21	6	15
Chipps Island	2.53	3.52	16	19	13	14	20	6	13
Sherman Island	2.79	3.66	16	16	12	13	20	7	16
Twitchell Island	3.47	4.56	11	14	9	16	23	12	13
Rio Vista	4.75	6.11	10	13	9	15	27	11	14
Vernalis	6.30	5.62	13	15	11	17	20	10	14
Garcia Bend	3.94	5.44	10	14	10	16	24	12	14

Table 13 2015 transect THNS concentrations, THNS carbon-normalized yields, and molar percentage of THNS (mol %).

Site Name	THNS ($\mu mol\ L^{-1}$)	THNS Yield (% OC)	Fuc	Rha	Ara	Gal	Glc	Man	Xyl
			(mol %)						
Golden Gate Bridge	0.74	3.66	22	15	7	22	14	8	13
San Pablo Bay	0.80	1.51	20	15	10	16	18	8	12
Benicia	1.12	2.67	15	14	9	15	23	10	14
Roe Island	1.23	2.66	16	15	9	14	19	12	15
Belden's Landing	1.77	3.51	17	15	11	15	18	10	14
Honker Bay	1.59	3.89	14	14	9	14	24	11	14
Chain Island	1.19	3.02	14	15	9	15	19	12	15
Sherman Island	1.40	3.92	13	14	9	15	24	11	14
Decker Island	1.17	3.45	16	15	9	16	17	11	15
Twitchell Island	1.63	4.40	16	14	8	16	20	10	15
Ida Island	1.78	7.65	17	15	7	17	18	12	13
Vernalis	2.39	8.32	23	13	6	16	18	13	11
Garcia Bend	1.60	7.31	18	15	7	17	16	12	15

Table 14 2016 transect THNS concentrations, THNS carbon-normalized yields, and molar percentage of THNS (mol %).

Site Name	THNS ($\mu mol\ L^{-1}$)	THNS Yield (% OC)	Fuc	Rha	Ara	Gal	Glc	Man	Xyl
			(mol %)						
Golden Gate Bridge	0.51	2.98	23	12	8	16	18	8	15
San Pablo Bay	1.39	4.60	11	9	6	12	42	7	14
Benicia	0.75	2.59	15	20	12	15	16	7	15
Lower Susan Bay	0.92	2.52	18	18	11	14	17	7	16
Roe Island	1.22	3.50	16	15	9	15	20	10	15
Honker Bay	1.38	4.02	15	15	8	14	25	6	18
Belden's Landing	3.40	3.41	18	15	11	15	16	5	19
Chain Island	1.78	5.30	15	13	6	16	28	9	12
Decker Island	1.60	5.22	16	15	7	13	26	6	16
Twitchell Island	1.76	4.38	13	13	8	13	29	9	15
Ida Island	1.34	5.23	15	16	8	16	22	9	14
Rio Vista	1.49	5.21	15	17	7	15	23	8	14
Vernalis	1.57	3.63	16	14	9	16	20	9	15
Garcia Bend	0.96	4.34	17	16	8	15	17	10	17

THAA carbon-normalized yields ranged from 1.69 to 6.10 % OC in 2014 and did not demonstrate a trend with salinity. THAA carbon-normalized yields were highest at Golden Gate Bridge, though Delta sites had higher THAA carbon-normalized yields than stations in the Bay (Table 15, Figure 14). The 2014 transect stations had elevated abundances of Gly and Asp (mol %), and Gly had the highest abundance in all sites ranging from 16.7-29.1 mol % (Table 15). Glu, Ser, His, Gly, and Ile had an increase in abundance through the transect. Thr, Arg, Ala, Val, Phe, Leu, and Lys demonstrated a decrease in abundance across the 2014 transect. In 2015, THAA carbon-normalized yields ranged from 1.69 to 12.84 % OC. Golden Gate and Garcia Bend had the highest THAA carbon-normalized yields, while Bay sites had lower THAA carbon-normalized yields than Delta sites (Table 16, Figure 14). Gly, Glu, Ser, and Ala were abundant in all stations in 2015 (Table 16). Gly was the most abundant amino acid in 2015 sites with a range of 21.2-34.3 mol%. Asp decreased with across the transect with the exception of similar abundances in Golden Gate and Belden's Landing compared Delta sites. Glu and Ser had a higher abundance in Delta stations than Bay stations except for station 1 (Table 16). In 2016, THAA carbon-normalized yields ranged from 0.88 to 10.23 % OC (Table 17, Figure 14).

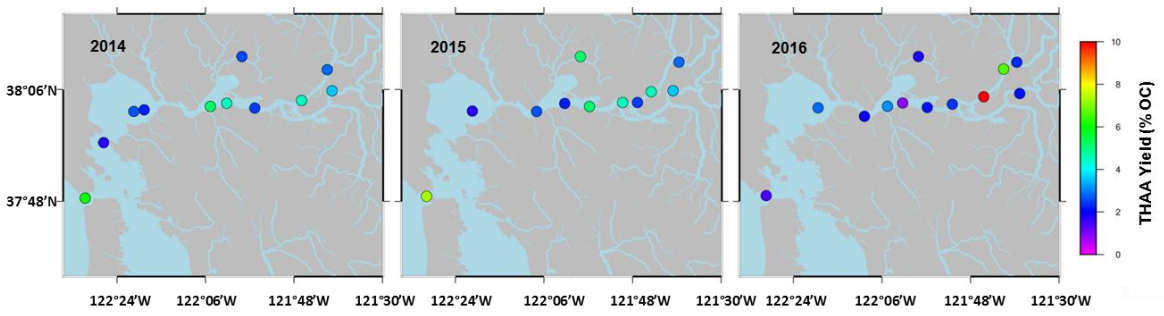

Figure 14 THAA yields (% OC) in the 2014, 2015, and 2016 transects.

Table 15 Transect samples from 2014 THAA concentrations, THAA carbon-normalized yields, mole percentage of D-amino acids (D-AA) (mol %), and relative abundance of THAA (mol %) composition of leachates.

#	Site Name	THAA	THAA Yield	D-AA	Asp	Glu	Ser	His	Thr	Gly	Arg	Ala	Tyr	Val	Ile	Phe	Leu	Lys
		(μmol L^{-1})	(% OC)	(mol %)	(mol %)													
1	Golden Gate Bridge	2.58	6.10	4.38	10.2	15.6	17.2	3.5	3.4	24.9	1.5	7.4	1.7	2.1	6.5	2.2	1.0	2.7
2	San Rafael Bay	0.76	1.69	2.44	15.5	9.6	7.7	1.6	4.8	29.1	1.0	7.9	0.8	0.0	18.5	2.0	0.0	1.5
3	San Pablo Bay	1.55	2.66	3.45	11.9	10.7	10.5	2.0	5.4	24.5	1.6	9.3	1.5	2.8	10.7	3.5	2.8	2.7
4	San Pablo Bay (Entrance)	1.57	2.22	3.92	13.2	10.9	10.9	1.7	5.5	23.3	1.3	9.7	1.3	3.0	10.6	3.5	2.5	2.5
5	Lower Susan Bay	4.49	5.17	6.65	9.9	12.3	15.4	2.5	5.6	21.8	2.0	9.4	2.1	3.9	5.1	3.3	3.6	3.2
6	Belden's Landing	4.20	2.56	5.76	11.2	7.4	7.0	0.8	5.8	23.3	2.6	9.6	1.7	7.0	4.9	5.5	10.1	3.1
7	Roe Island	4.55	4.51	5.54	9.3	12.7	17.2	2.3	5.8	21.5	1.6	10.2	1.7	3.9	4.8	3.1	3.2	2.8
8	Chipps Island	2.50	2.48	4.35	11.8	10.2	10.8	0.9	6.6	22.0	1.6	11.2	1.4	4.7	7.9	3.9	4.4	2.7
9	Sherman Island	4.87	4.52	6.86	9.5	12.6	15.3	1.2	5.9	22.0	2.0	10.1	1.8	4.3	4.9	3.6	3.9	2.9
10	Twitchell Island	3.47	3.58	5.37	9.7	8.0	8.0	0.7	5.7	18.6	3.1	9.1	1.7	7.9	5.9	6.3	11.9	3.4
11	Rio Vista	2.70	2.84	4.32	10.1	6.2	5.6	0.5	5.9	16.7	3.3	9.0	1.9	8.9	7.1	7.2	14.2	3.5
12	Vernalis	5.04	3.34	11.45	12.1	7.9	6.4	0.5	6.3	22.4	2.7	10.6	1.1	7.0	4.6	5.4	9.6	3.3
13	Garcia Bend	3.58	3.97	17.05	10.0	7.2	5.9	0.6	6.2	17.4	3.2	9.5	1.8	8.5	6.2	6.9	13.0	3.5

Table 16 Transect samples from 2015 THAA concentrations, THAA carbon-normalized yields, and relative abundance of THAA (mol %) composition of leachates.

#	Site Name	THAA	THAA Yield	D-AA	Asp	Glu	Ser	His	Thr	Gly	Arg	Ala	Tyr	Val	Ile	Phe	Leu	Lys
		(μmol L^{-1})	(% OC)	(mol%)	(mol %)													
1	Golden Gate Bridge	2.13	7.32	4.17	11.9	9.6	8.3	0.5	7.7	23.4	1.1	12.3	0.5	5.6	9.5	3.4	4.0	2.2
2	San Pablo Bay	0.64	1.69	0.73	4.9	15.8	17.5	2.9	4.0	23.4	2.6	11.3	1.2	2.1	7.5	2.9	4.0	0.0
3	Benicia	0.63	2.66	1.57	4.4	6.7	6.4	2.4	2.1	33.4	1.4	14.3	1.5	2.5	17.6	2.2	3.9	1.2
4	Roe Island	1.12	2.22	1.76	4.3	7.5	11.8	1.9	3.1	30.5	2.4	14.1	0.9	3.4	12.1	2.6	4.4	0.7
5	Belden's Landing	3.80	5.11	13.20	12.9	8.3	7.1	0.5	7.6	25.9	1.0	13.5	0.2	4.8	10.0	3.1	3.0	2.1
6	Honker Bay	1.51	5.17	2.27	4.2	8.4	9.0	1.4	3.2	34.3	1.9	14.1	0.6	3.6	10.0	2.5	4.4	2.3
7	Chain Island	3.08	4.51	2.39	5.5	13.7	16.4	0.8	4.5	27.7	1.6	12.5	0.3	3.5	5.8	2.2	3.6	1.8
8	Sherman Island	3.59	2.48	2.07	6.6	14.5	18.6	1.0	5.5	24.6	1.4	12.4	0.3	3.4	4.9	2.0	3.0	1.8
9	Decker Island	2.43	4.52	3.50	9.3	10.0	12.0	1.2	6.3	28.4	1.0	12.8	0.4	3.9	7.2	2.3	3.8	1.4
10	Twitchell Island	2.62	3.58	2.60	9.0	14.9	16.9	0.9	5.8	21.2	1.5	11.1	0.6	4.4	4.8	2.9	3.7	2.4
11	Ida Island	2.47	2.84	5.45	11.0	10.2	10.2	0.5	7.4	23.9	0.9	12.9	0.4	5.0	9.2	3.0	3.3	2.0
12	Vernalis	2.40	5.68	5.85	12.3	8.7	8.1	0.4	8.3	23.8	1.1	13.4	0.5	6.1	8.0	3.3	3.8	2.3
13	Garcia Bend	4.20	12.84	14.79	11.1	7.6	7.9	0.9	6.8	29.3	0.9	11.8	0.6	4.0	11.7	2.8	2.8	1.8

Table 17 Transect samples from 2016 THAA concentrations, THAA carbon-normalized yields, and relative abundance of THAA (mol %) composition of leachates.

#	Site Name	THAA	THAA Yield	D-AA	Asp	Glu	Ser	His	Thr	Gly	Arg	Ala	Tyr	Val	Ile	Phe	Leu	Lys
		(μmol L^{-1})	(% OC)	(mol %)	(mol %)													
1	Golden Gate Bridge	0.32	1.43	1.28	15.8	16.0	6.3	2.4	7.0	17.3	3.2	11.6	2.2	10.2	NA	7.9	NA	0.0
2	San Pablo Bay	1.15	2.84	3.04	16.6	16.0	6.9	1.9	5.6	16.0	2.9	13.3	2.6	6.8	NA	6.0	NA	5.4
3	Benicia	0.72	1.87	2.23	16.5	10.0	7.0	1.7	6.8	18.7	3.2	13.8	2.1	7.4	NA	8.8	NA	4.1
4	Lower Susan Bay	1.59	3.13	5.05	15.3	10.2	8.2	1.3	7.1	18.7	2.8	17.0	2.3	7.0	NA	6.0	NA	4.1
5	Roe Island	0.41	0.88	1.40	14.8	13.5	5.3	2.5	8.4	17.1	4.2	13.0	2.7	8.4	NA	5.6	NA	4.4
6	Honker Bay	1.03	2.14	2.38	13.5	11.3	9.1	1.6	8.0	19.2	1.9	16.6	2.2	6.9	NA	5.9	NA	3.8
7	Belden's Landing	2.57	1.75	8.52	15.3	9.8	10.0	0.9	8.0	21.2	2.0	18.6	1.7	5.3	NA	4.2	NA	3.0
8	Chain Island	1.15	2.41	2.17	13.7	11.8	9.4	1.4	8.2	18.4	1.4	17.1	1.9	6.9	NA	5.9	NA	3.9
9	Decker Island	3.55	10.23	3.65	4.1	14.3	4.2	0.4	5.9	7.9	8.9	17.0	4.2	14.7	NA	13.6	NA	4.9
10	Twitchell Island	1.16	2.09	1.05	12.0	10.9	10.8	2.3	7.3	16.7	4.3	13.9	1.9	6.2	NA	5.1	NA	3.5
11	Ida Island	0.81	2.32	1.38	13.5	14.7	8.6	1.7	7.9	16.7	4.6	14.1	2.0	6.5	NA	6.0	NA	3.8
12	Rio Vista	2.70	6.64	1.70	9.0	7.0	20.4	4.2	7.9	16.5	3.8	14.4	2.1	5.7	NA	5.7	NA	3.3
13	Vernalis	1.11	1.79	1.64	14.0	10.5	9.4	1.2	7.8	19.9	3.7	16.7	1.9	6.6	NA	4.5	NA	4.0
14	Garcia Bend	1.05	3.52	1.53	13.4	12.1	9.0	1.3	7.4	15.7	4.1	16.2	2.5	7.7	NA	5.8	NA	4.7

D-AA molar abundance in 2014 ranged from 2.44 to 17.05 mol % (Table 15). D-AA abundance was highest in the riverine stations Garcia Bend and Vernalis, with variability throughout the Delta and Bay (Table 15). The 2015 transect had D-AA that ranged from 0.73 to 14.79 mol % and was elevated at Belden's Landing and Garcia Bend, the Sacramento River endmember (Table 16). D-AA molar abundance in the 2015 transect ranged from 0.73 to 14.79 mol % and did not have a trend with salinity. The 2016 transect D-AA molar abundance ranged from 1.05 to 8.52 mol % (Table 17). D-AA abundance for 2016 was low in the Delta with higher abundance at Belden's Landing and Susan Bay. D-AA abundance was higher in the Bay in 2014 than in 2015 and 2016. The transect collected in 2016 had the lowest D-AA molar abundance in the river endmembers. 2014 had the highest abundance of D-AA (mol%) in both river endmembers. Carbon-normalized D-AA concentrations in the 2014 transect ranged from 20-50 nmol mg C^{-1} (Figure 15). In the 2015 transect, concentrations of carbon-normalized D-AA ranged from 0-75 nmol mg C^{-1}, and concentrations in the 2016 transect ranged from 10 to 50 nmol mg C^{-1} (Figure 15). The 2015 transect had the largest range of D-AA carbon-normalized concentrations with low concentrations in the Delta and through Suisun Bay, but hotspots in localized stations.

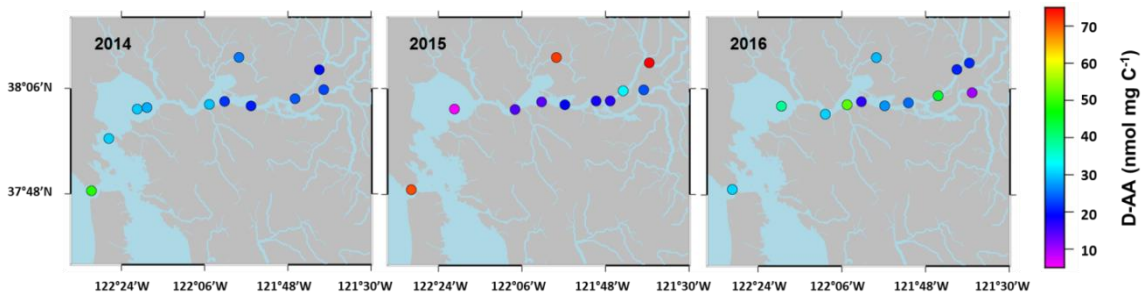

Figure 15 Carbon-normalized D-AA concentrations in the 2014, 2015, and 2016 transects.

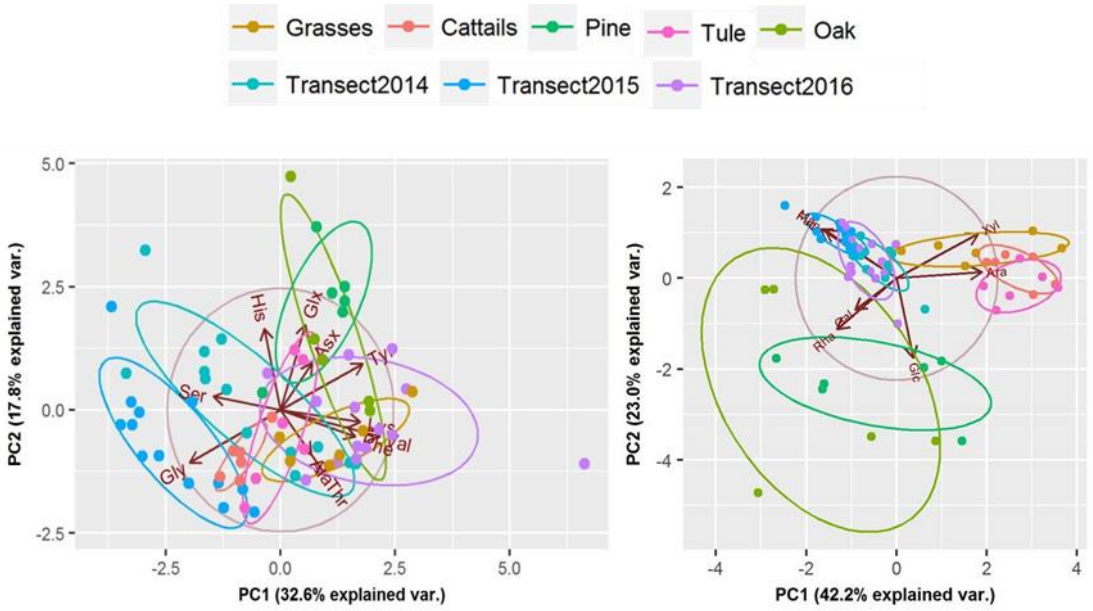

Figure 16 Principal component analyses (PCA) of relative abundance of THAA and relative abundance of THNS for all coupled incubation time points and 2014, 2015, and 2016 transect samples. A 95% confidence ellipsis was applied to describe the region where 95% of the time a new point would be estimated.

Principal component analysis of neutral sugars showed distinct compositional differences in the incubations (grasses, cattails, and tule versus pine and oak) and in the transects from the incubations (Figure 16). The abundance of neutral sugars shifted from Glc and Xyl to Fuc (Figure 16). All transects were enriched in Fuc. There was no compositional distinction in the neutral sugars of the three transects. Grasses, cattails, and tule were enriched in xylose while pine and oak were enriched in glucose. The distinctions in THNS composition for the incubations were detailed in section 3.2. of the Results. The principal component analysis of THAA molar abundance in the transects and incubations did not yield clear distinctions on potentials sources for DOM in transect samples (Figure 16). Gly was enriched in the 2015 transect.

Labile in situ DOC and labile terrestrial DOC (tDOC) were calculated for natural samples using the equations produced by Davis and Benner (2007). Labile in situ DOC was calculated from amino acid carbon-normalized yields (Davis and Benner, 2007).

The 2014 transect had labile in situ DOC between 0 to 21 % total DOC and was high at the marine endmember and elevated in some of the Delta-Bay sites (Figure 17). In 2015, labile in situ DOC ranged from 0 to 27 % total DOC with elevated labile in situ DOC at the marine endmember. The transect in 2016 ranged from 0 to 6 % total DOC with two stations that had >23 % total DOC (Figure 17). Labile in situ DOC made a higher percentage of the total DOC in 2014 and 2015 samples than in 2016.

Labile tDOC ranged from 2 to 25 % total DOC in the 2014 transect, from 0 to 35 % total DOC in 2015, and 1 to 19 % total DOC in 2016 (Figure 17). Labile tDOC made a higher percentage of the total DOC at the Delta stations than the Bay stations in all three transects. The 2014 and 2015 transects had Delta stations with high percentages of labile tDOC. However, the 2016 transect had elevated percentages of labile tDOC at all Delta stations (Figure 17).

High regime flow had higher labile tDOC percentages (~20%) in the two rivers than the low flow (~10%), but record low flow had the highest labile fraction of tDOC (~35%) in the riverine endmembers. Labile in situ DOC in the riverine endmembers was similar (~10%) in the Sacramento River (Garcia Bend) for high flow (2014) and low flow (2016) while the San Joaquin River (Vernalis) had 7% of total DOC composed of labile in situ fraction in the high flow during 2014 and 0 % in the low flow in 2016. Record low flow in 2015 had much higher values (19% in Vernalis and 55% in Garcia Bend) of labile in situ DOC than either high or low flow regime. During record low flow, over 50% of the DOC in the San Joaquin River was characterized as labile (both tDOC and in situ) and almost 90% was characterized as labile in the Sacramento River. During high flow, approximately 30% was characterized as labile in both rivers, and during normal low flow regime in 2016, 10% in the San Joaquin River and 22% in the Sacramento River was characterized as labile.

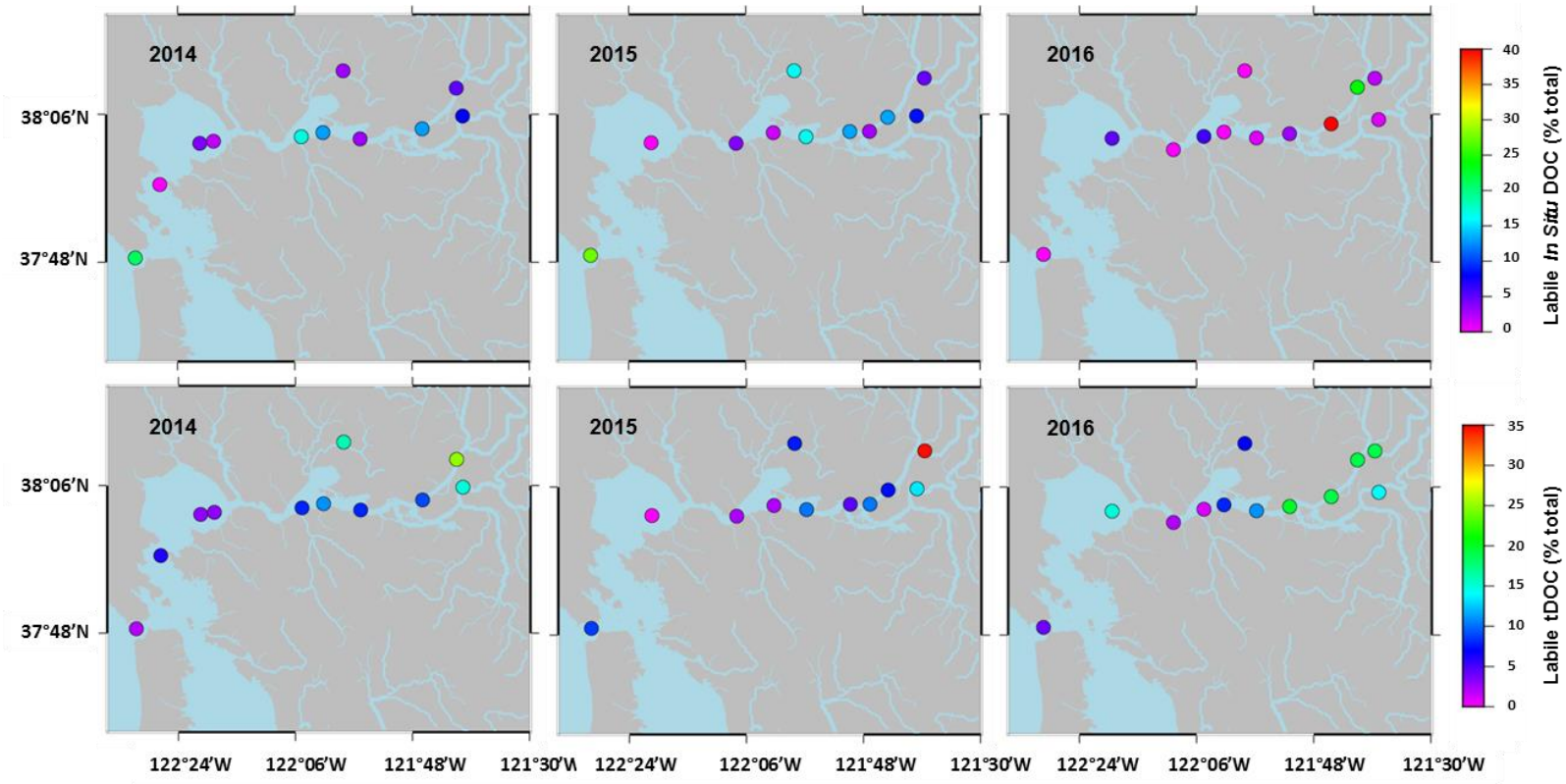

Figure 17 Labile in situ DOC (% total) and tDOC (% total) in transects. Labile in situ DOC was calculated using the equations produced by Davis and Benner (2007).

4. DISCUSSION

4.1 Factors Affecting Leachate Composition of Litters

Inquiries into the leaching of material from plants have been pursued as far back as de Saussure's 1804 experiments with washed leaves. Since then, many experiments have worked to determine the effects of leaching, factors that influence leaching, and possibly most importantly the compounds leached from plant material. Leaching processes occur on metabolites in the plant as opposed to structural material. Leaching mobilizes soluble secondary components.

Plant material is more susceptible to leaching with age. Senescent plant material leaches higher quantities of soluble compounds than younger, growing plant material (Tukey, 1970). Furthermore, plants with waxy coating covering the leaves are more resistant to leaching (Tukey, 1970). Leaching results in large losses of mass and compounds in plants and releases key nutrients such as carbon, nitrogen, and phosphorous. Aromatic compounds are prevalent in fresh plant material and form soluble secondary products, some aromatic amino acids, and lignin that are easily leached from plants (Fuchs et al., 2011). Tannins are a polyphenolic compound in oak that are highly soluble. Other important compounds leached from plant material include amino acids and neutral sugars from cellulose and hemicellulose.

The vascular plants leached for this experiment were chosen due to their prevalence in the San Francisco Bay/Sacramento-San Joaquin River Delta estuary. Each vascular plant type was ground to litter and leached for 24 hours in the dark in Milli-Q water. During leaching, ~4-26% of the available organic carbon in each litter type was soluble under these conditions (Table 3). Maie et al. (2006) determined a two-step process to the leaching of DOM from vascular plants (cut to ~8 cm length) during a prolonged leaching incubation of key wetland plants dominant in the Florida Everglades. They determined first a rapid release of components occurs with a half-life of 1-4 days followed by a slower release of 19 days or more (Maie et al., 2006). Nykvist (1963) determined environmental temperature, level of decomposition, and structure influenced

the leachability of different litter types. Furthermore, how finely ground the litter is can significantly increase the amount of water-soluble organic substances leached (Nykvist, 1963). In this experiment, vascular plant material was ground to pass through a 350-µm sieve, which should have enabled a significant portion of the plant components to be rapidly released.

The soluble fraction of organic carbon in the vascular leachates was highest in pine and oak litters, 12.2 % OC and 25.8 % OC respectively. The soluble fractions for grasses, cattails, and tule were only ~4% of the organic carbon of the litter. The difference in solubility of the organic carbon in the litters could be influenced by the structural components of the litter compared to secondary soluble products. THAA (% OC), THNS (% OC), and aromaticity (% OC) composed 27-35% of the soluble fraction in these five vascular plant leachates (Table 3). Leachates in this study had higher THNS carbon-normalized yields (8.4-16.9 % OC) than THAA carbon-normalized yields (0.6-4.1 % OC). Opsahl and Benner (1999) found neutral sugar carbon-normalized yields ranged 8.5-26.8% of the plant tissue carbon in their vascular plant samples. The THNS carbon-normalized yield (8.4-16.9 % OC) of our soluble fraction of DOC falls within that range. Neutral sugars were a significant component of the DOM of the vascular plants used in this study. Mixed grasses litter yielded the highest THAA carbon-normalized yield in the soluble fraction, and pine and mixed grasses litters had the highest THNS carbon-normalized yields (Table 3). Cowie and Hedges (1994) determined THAA carbon-normalized yields were low in wood-type plants or amino acids were preferentially degraded compared to other organic compounds, which our findings support (Table 3). Oak leachate had the highest aromaticity (21.6 % OC) of the five vascular plant leachates.

Glucose was not enriched in leachates, which suggested secondary hemicelluloses dissolved during leaching (Table 7). Initial D-AA (mol %) in the leachates indicated input from bacterial DOM was already present at the beginning of the incubations and suggested amino acids were derived from bacteria in addition to plant protein. D-AA is contained in the cell walls of bacteria, and soil bacteria have

thicker cell walls than other microbial communities (Kaiser and Benner, 2008). Higher initial D-AA in initial leachate samples supports the presence of bacterial communities coating the surface of the vascular plant litters before the incubation experiments began.

4.2 Changes in Chemical and Molecular Composition during Decomposition of Leached Material

Initial loss of DOC occurred rapidly in all vascular plant leachates (Table 4, Figure 5); indicating decomposition by microbial and photochemical processes (Miller and Moran, 1997; Kawasaki and Benner, 2006; Gruber et al., 2006). Vascular plant leachates lost >50% of the initial DOC by the end of the incubations. Cattails leachate DOC showed a more gradual decline during the incubation possibly due to the presence of DOM pools with varying reactivities. The timescales used in these incubations did not enable to resolve multiple pools of decomposable DOM, and further investigation would be needed to determine the cause of resistance to degradation seen in the cattails leachate. On the same time scale as cattails, oak leachate demonstrated resistance to degradation. The oak and tule leachate incubations had longer time frames which encouraged further degradation and/or alteration of DOM. However, these longer incubations did not as accurately reflect the residence times these leachates would encounter in a natural system such as the Sacramento-San Joaquin Delta/ San Francisco Bay estuary. The grasses leachate lost >80% of initial DOC during the incubation, which indicated the constituents of grasses DOM were highly labile under coupled photochemical and microbial processes. A loss of aromaticity indicated decomposition of the DOM through photodegradation or microbial degradation. However the rate of decay and increase of aromaticity in the % total of DOC demonstrated resistance of semi-labile or refractory aromatic compounds to degradation (Table 5, Figure 6).

Aromatic DOM is the most photoreactive component in DOM (Osburn et al., 2001; Weishaar et al., 2003; Stubbins et al., 2008; Helms et al., 2014). Under coupled incubation conditions, aromaticity (%OC) increased. The decay rate of aromaticity was slower than neutral sugars and DOC for all leachates. Carbon-normalized aromaticity

reflected removal of aromatic carbon through photochemical degradation during incubations, but the percent aromaticity of the organic carbon in the leachates increased throughout the incubations. Aromatic carbon in these samples was largely refractory on the timescales of the coupled incubations. Previous studies used experimental decay models to determine 54-69% of aromatic-rich tDOC was photorefractory (Moran et al., 2000; Obernosterer and Benner, 2004; Spencer et al., 2009; Vähätalo and Wetzel, 2004).

During photochemical processes, $S_{275-295}$ increases and $S_{350-400}$ decreases, which results in an increasing S_R and reflects photodegradation of CDOM (Helms et al., 2008; Helms et al., 2013). Previous studies determined photochemical processes induce increases in slope ratio while microbial degradation decreases slope ratio (S_R) values (Moran et al., 2000; Vähätalo and Wetzel, 2004; Helms et al., 2008). Terrestrially derived DOM is characterized with $S_{275-295} < S_{350-400}$ while marine DOM has $S_{275-295} > S_{350-400}$, which characterizes S_R values <1 as indicative of terrestrial material and S_R values >1 indicate a marine signature (Helms et al., 2008) or decomposed and transformed material. UV slope values for coastal CDOM at wavelength 275-295 ($S_{275-295}$) normally fall between 10 to 20 μm^{-1} for terrestrially derived material (Helms et al. 2008; Fichot and Benner, 2012). Marine CDOM signatures have higher S values of about 20 to 30 μm^{-1} (Stedmon et al., 2011). In incubation samples, leachates in this experiment had $S_{275-295}$ within the range for terrestrially derived material found by Helms et al. (2008) and Fichot and Benner (2012) except the pine leachate (Table 4). The S_R values for grasses, cattails, and tule all shifted from a terrestrial DOM signature to a marine signature. The increasing spectral slope coefficient of absorbance from 275 to 295 nm throughout the duration of the incubations in grasses, cattails, and tule leachates reflected a shift from terrestrial DOM to reworked microbial DOM (Table 4). Pine and oak leachates' $S_{275-295}$ value decreased from the initial to the end time points. Pine and oak leachates had a marine signature (S_R >1) that decreased throughout the incubations. $S_{275-295}$ and S_R indicators for pine and oak coupled with other terrestrial/microbial indicators mentioned later in this discussion revealed a possible incorporation of microbial DOM in initial vascular plant leachates.

The fluorescence index (FI) uses the optical properties of DOM as an indicator of source to distinguish terrestrial (FI of ~1.4) versus microbial (FI of ~1.9) origin (McKnight et al., 2001; Cory and McKnight, 2005). Grasses, cattails, and tule had initial fluorescence index values that indicated terrestrial origin (Table 4). FI values had little change with time in cattails during the coupled incubations, which indicate the terrestrial dominance in the DOM signature throughout the incubation. FI values increased with time during the coupled incubations for grasses and tule as there was a shift from terrestrially derived DOM to microbially derived DOM (Table 4). Pine had a very large FI value (2.13) initially indicating microbial predominance of the DOM. However, during the pine incubation, the FI value was a terrestrial signature (1.4) and shifted to a microbial signature (2.23) (Table 4). Oak time points had decreasing FI values over time with a higher microbial signature (>1.9) initially and a shift to terrestrial dominance in the FI value (Table 4). Due to the presence of microbial communities coating the surface of the leaves, a higher presence of microbial DOM in the initial samples of Pine and Oak could have influenced the FI signature.

The biological/autochthonous index (BIX) is applied to determine the contribution of autochthonous productivity to DOM used to characterize DOM in estuarine systems (Huguet et al., 2009; Walker et al., 2013). Low BIX values (<1) indicate low abundance of biologically derived DOM, while values >1 indicate autochthonous biologically derived DOM (Huguet et al., 2009). Birdwell and Engel (2010) determined a BIX value of 0.8-1.0 indicated microbially derived DOM, and allochthonous sources had a BIX value < 0.6. Based on this index, grasses had the greatest contribution of microbially derived DOM throughout the coupled incubations (Table 4). Oak had the lowest contribution of microbially derived DOM as indicated by the BIX values (Table 4) supported by low abundances of D-AA and Gly, high abundance of Glc, and slow loss of DOC, as discussed in previous sections. Oak leached DOM was more resistant to microbial decomposition than other leachates.

Preferential decay of neutral sugars occurred in all vascular plant leachates (Table 5, Figure 5), which suggests neutral sugars are more labile than bulk DOC and

aromatic compounds. THNS is one of the more reactive components of DOM that is rapidly degraded in the early stages of diagenesis, and the most rapid removal occurred before the 20 day mark in our incubations. Carbon-normalized yields of neutral sugars are a reliable index of DOM degradation (Cowie and Hedges, 1994; Skoog and Benner, 1997; Amon et al., 2001; Kaiser and Benner, 2009). The largest loss of THNS carbon-normalized yields occurred early in the incubations for all leachates. Grasses, cattails, and pine leachates carbon-normalized THNS yields increased late in the incubations. This could occur due to degradation of a different constituent of the DOC for these leachates that caused the remaining THNS concentration to compose a larger percentage of the remaining DOC. Oak leachate had a gradual change in the percent of organic carbon composed of neutral sugars in the start of the incubation before the THNS carbon-normalized yield reflected the plateau seen in DOC loss. Tule was the only leachate in this experiment that demonstrated a loss of neutral sugars throughout the incubation and had the most removal of neutral sugars with only 1% OC composed of neutral sugars at the end of the incubation.

Glucose is a highly abundant neutral sugar in vascular plants occurring in structural polymers such as cellulose and hemicelluloses (Moers and Larter, 1993; Opsahl and Benner, 1999). Glucose abundance in DOM is considered a useful indicator of the extent of degradation (Moers and Larter, 1993). Loss of glucose abundance in leachates during initial time points mirrored the initial rapid decrease and then more gradual decline of THNS concentrations (Table 7, Figure 5). However, the tule leachate demonstrated extensive loss of DOC (Table 4) during the incubation that was not reflected in the increase of glucose relative abundance during the incubation (Table 7). It is possible under the conditions of the tule incubation the neutral sugars including glucose remained the preferentially degradable components of the DOC.

Opsahl and Benner (1999) found vascular plants abundant with arabinose, rhamnose, mannose, and galactose, and in angiosperms, xylose can be found in abundance. Our data indicated glucose is an abundant neutral sugar in leachates of vascular plants, prevailing in pine and oak, but xylose abundance was elevated in grass

type leachates (grasses, cattails, and tule) with molar abundances as significant as or even higher than glucose in some instances (Table 7). Principal component analysis of neutral sugars showed distinct compositional differences in the incubations of grasses, cattails, and tule versus pine and oak based on the enrichment of Xyl and Ara or Glc respectively (Figure 8). These results suggest grasses, cattails, and tule are enriched in hemicellulose while pine and oak are enriched in cellulose. This analysis indicates a potential compositional difference between the grass type vascular leachates and tree type leachates that may contribute to distinguishing not only sources, but relative input from these sources (Cowie and Hedges, 1984). Fucose was found to have a low abundance in vascular plants leached (Opsahl and Benner, 1999). Our data reflected these findings (Table 7). Fucose abundance was low in initial time points and increased during the incubation period, which can be contributed to microbial input to the DOM in this study (Aspinall, 1983; Moers and Larter, 1993).

The most labile neutral sugars are glucose and xylose (Opsahl and Benner, 1993, 1999). Moers and Larter (1993) suggested glucose, xylose, and rhamnose are the preferentially utilized neutral sugars. In our vascular plant incubations, glucose and xylose abundance did decrease preferentially over the course of the incubations in leachates, but rhamnose abundance increased in all leachates except oak, which had a decrease in later time points in relative abundance (Table 7).

Amino acids are another component of DOC that are preferentially degraded or altered in the early stages of diagenesis (Coffin, 1989; Keil and Kirchman, 1993; Cherrier and Bauer, 2004; Davis and Benner, 2007; Davis et al., 2009). THAA carbon-normalized yields are reliable indicators of diagenesis (Cowie and Hedges, 1994; Benner and Kaiser, 2003; Kaiser and Benner, 2008; Kaiser and Benner, 2009). Vascular plant leachates in this study had low THAA carbon-normalized yields throughout incubations (~0-4 %OC). Initial carbon-normalized THAA yields decreased rapidly in the first time points of each vascular plant leachate. The principal component analysis on THAA molar abundance in these leachates revealed a large distinction in the amino acid composition of pine and oak leachates versus mixed grasses, cattails, and tule leachates

(Figure 8). Oak had the largest shift in amino acid composition over the course of the incubation while cattails composition changed very little during the incubation (Figure 8). Increasing glycine abundance indicates degradation (Yamashita and Tanoue, 2003), and glycine molar abundance in all leachates increased during incubations with the exception of oak (Table 6).

D-enantiomers of the amino acids (D-AA) Asx, Glx, Ser, and Ala are found in the cell wall of bacteria and are useful indicators of input from bacterial derived DOM (Kawasaki and Benner, 2006). D-AA (mol %) abundance in grasses, cattails, pine, and tule leachates increased over time and indicated microbial degradation (Table 6). Kaiser and Benner (2008) and others found D-AA reactivity reflects reactivity of bacterial carbon and is an accurate biomarker for bacterial DOM contributions.

The combined effect of microbial and photochemical decomposition on vascular plant leachates yields a larger processing and degradation of leachate DOM than either process could alone. Photochemical decomposition affected colored biomolecules like aromatic carbon in DOM while microbial decomposition preferentially targeted biolabile molecules such as neutral sugars and amino acids. Photochemical alterations produce photoproducts that are more bioavailable, fueling microbial degradation of previously biorefractory components (Kieber et al. 1989; Miller and Moran, 1997).

4.3 Cycling of Dissolved Organic Matter in San Francisco Bay and Delta

The collection of samples was geared toward describing the system during different seasons and flow regimes. A winter transect in December 2014 at high riverine discharge was collected to study the DOM dynamics largely in the absence of photodegradation processes and low levels of algal production. A transect was collected in June of 2015 when drought conditions were observed and the water flow was very low. A second summer transect was taken in May of 2016 to sample significant photodegradation and algal production conditions in the Delta-Bay. Sampling was done for all transects with a riverine endmember for the San Joaquin and Sacramento River

respectively, with higher density sampling at low salinities taken across an axial transect from river to coastal ocean (Figure 4).

The San Francisco Bay is a tidal-influenced environment. During seasonal low inflow of freshwater from the Delta, higher salinity water from the Pacific is drawn into the Bay and Delta (Murrell and Hollibaugh, 2000). This intrusion causes salinity levels in the Delta to reach 0.1 to 6 PSU (Figure 10). Salinity was highest in Suisun Bay and the lower Delta during the record low flow in 2015, while the low flow regime had salt water intrusion up to the beginning of the connection through Suisun Bay, at the end of the Delta. During the high flow regime (2014), the Suisun Bay experienced salt water intrusion, but the lower Delta and connection to Suisun Bay did not (Figure 10).

Seasonal flow affects freshwater and associated DOM input from the Delta to the Bay. A downward trend occurs spring to late summer (~April to November) through June and an upward input trend from winter to spring (December to March) (Fox et al., 1990; Murrell and Hollibaugh, 2000; Enright and Culberson, 2009). The seasonal riverine inflow during summer through autumn can drop as low as ~100 m^3s^{-1} and during the wet season in winter surge >9000 m^3s^{-1} (Murrell and Hollibaugh, 2000; Cloern and Dufford, 2005). The residence times in Suisun Bay, San Pablo Bay, and San Francisco Bay experience variability due to season. Walter et al. (1985) found residence times in these areas were on timescales of days during high flow regime in the winter and timescales as long as months during low flow regime in the summer. Between the years of 2012 and 2016, California was under severe drought conditions and record breaking temperatures, and in late 2015 and early 2016 experienced a strong El Nino event. However, riverine discharge to the estuary, in situ inputs of DOM, and the dynamics of the Delta-Bay are arguably most important in the flux, composition, and fate of the riverine DOM.

Winter season conditions include high riverine discharge, DOM and nutrient input from flushing events, low levels of algal production, and limited photodegradation processes. The summer season conditions in the Delta-Bay are in general characterized by low riverine discharge, low outflow from the Delta to the Bay, high in situ (algal)

production, and significant photodegradation. The winter transect (2014) and the summer transects (2015 and 2016) reflect these seasonal characteristics in the concentration and composition of DOM. DOC concentrations seasonally vary in the Delta-Bay by decreasing from the summer up to the winter when increased precipitation and riverine flow cause increased DOC concentrations (Eckard et al., 2007). Flushing of terrestrial DOM into the Sacramento-San Joaquin River Delta caused elevated DOC concentrations (Table 9, Figure 11). The 2015 and 2016 summer transects reflected low discharge, higher productivity conditions in lower DOC concentrations, (Table 10, Table 11, Figure 11).

The 2014 transect was collected during higher inflow, lower productivity dynamics in the Delta-Bay compared to the lower inflow, higher productivity conditions of the summer collections in 2015 and 2016. Therefore, DOC concentrations in the 2014 transect were higher at stations further inland in the Delta compared to 2015 and 2016 transect stations due to high inflow of tributary loaded waters and low productivity in the Delta. Low inflow of waters into the Delta-Bay area give longer hydraulic dynamics and enable primary production, recycling DOC input from external riverine input into phytoplankton biomass (Jassby and Cloern, 2000). DOC concentrations for seasonally low freshwater input conditions in the Delta and Bay ranged from ~50 to 280 μM. but have not been well established due to limited sampling (Schemel, 1984; Kuwabara and Luther, 1993; Hunter and Kuwabara, 1994; Sanudo-Wilhelmy et al., 1996; Murrell and Hollibaugh, 2000). Variations in DOC concentrations collected on different years could be due to changes in input factors including seasonal precipitation, agricultural land drainage, waste discharge, outflow from the Delta, and tidal flow (Murrell and Hollibaugh, 2000; Hernes et al., 2006; Spencer et al., 2007; Oh et al., 2013).

The distribution of aromatic DOC showed complex patterns during high and low flow regimes. Aromaticity during high flow in 2014 was strongly attenuated along the salinity gradient. Aromatic carbon concentrations were much higher in river endmembers in the 2014 winter transect than the summer transects, due to the tributary loading and influx of more terrestrial plant-derived DOM. The low flow regime (2016)

showed high aromatic content throughout the estuary and a gradual decline from the Delta to Suisun Bay, but not in the Bay. Record low flow in 2015 showed lower aromatic content in the Delta and Bay compared to the 2014 and 2016 transects.

Optical proxies have been used to better understand both photochemical and microbial effects on DOM in aquatic systems (Moran et al., 2000; Stubbins, 2001; Vähätalo and Wetzel, 2004; Helms et al., 2008; Tzortiou et al., 2011). Previous focus on estuarine dynamics observed the shift of DOM from a terrestrial signature towards a marine signature (Stubbins, 2001; McCallister et al., 2006; Helms et al., 2008).Photochemical processes, microbial processes, intrusion or mixing of marine waters with freshwater, or a combination of these processes can affect optical properties of DOM in coastal estuary areas (Helms et al., 2008). Specifically, photochemical processes caused increased S_R values, and microbial processes caused a smaller, but significant decrease in S_R values (Helms et al., 2008). Helms et al. (2008) found shifts in S_R correlated with shifts in molecular weight in the Delaware estuary, and upriver samples had a lower, terrestrial S_R value (~0.71) while downriver and bay samples had a higher, estuarine S_R value (>1).

Each transect collected for this study had S_R values that support the findings of these previous studies (Tables 9, 10, 11). The 2014 winter transect during terrestrial-rich riverine inflow to the Delta-Bay had low S_R (ranging 0.71 to 0.76) freshwater at upstream stations and increasing S_R values (0.77-0.96) in higher salinity Bay waters (Table 9). The 2015 and 2016 summer transects had overall higher estuarine S_R values due to low riverine discharge conditions. Increasing $S_{275\text{-}295}$ and S_R in the 2014 winter transect demonstrate a shift in terrestrial signature to marine signature across the Delta to the Bay (Table 9). The 2016 transect shows a more terrestrial signature for one riverine endmember (seen in $S_{(275\text{-}295)}$ and slope ratio values) and begins to shift to marine signature further out in the Bay. The 2015 and 2016 transects had values close to a marine signature over terrestrial overall, but had little variation between samples. Tzortiou et al. (2011) used S_R to determine photodegradation of labile marsh-DOM was the dominant process in the Rhode River estuary during short time-scales, and microbial

degradation was a key process in mineralization of marsh-DOM on larger timeframes. While changes in $S_{275\text{-}295}$, S_R, and $SUVA_{254}$ appeared to reflect estuarine changes of terrestrial DOM composition and molecular size in 2014, in the 2015 and 2016 transects, changes in S_R did not seem to be driven by decreasing molecule size indicated by increasing $S_{275\text{-}295}$ (Weisharr et al., 2003; Helms et al., 2008). Changes in the molecular size and composition of the riverine DOM in the 2014 transect were probably driven by photodegradation and microbial degradation on a smaller level (Stubbins, 2001; McCallister et al., 2006; Helms et al., 2008). The summer transects would not have a S_R reflecting changes in $S_{275\text{-}295}$ since they are characterized by lower DOC concentrations with more in situ (biolabile algal) production, and more likely the S_R reflects the mixing of low -SR freshwater with high-S_R marine water.

All FI values for transects are between terrestrial and microbial values. While FI is a useful index for determining DOM sources, application of this index cannot distinguish between microbial or photochemically degraded sources (Moran et al., 2000; Spencer et al., 2009). McKnight et al. (2001) found low FI values indicating a terrestrial source in the Delta, which is likely due to lower phytoplankton production in the Delta from light-limited conditions (Jassby et al., 2002; Stepanauskas et al., 2005). In the 2014 transect, some sites had a BIX that was much closer to allochthonous than microbial in value (Table 9). 2015 and 2016 transects had BIX values closer to the range of microbial (Table 10 and 11) likely due to seasonal low flow input during those sample collections, which delivered already microbially degraded DOM to the system.

Amino acid and neutral sugar yields are more robust indicators of diagenesis for natural substrates in seawater as opposed to amino acid or neutral sugar compositions (Davis et al., 2008; Kaiser and Benner, 2009). THAA and THNS carbon-normalized yields in this study overall were better indicators of diagenesis through the Delta-Bay transects (Table 12, 13, 14, 15, 16 and 17). THNS Yields during high flow regime were higher in the Delta, lower in the Bay and reflected removal from the Delta and Bay. During low flow, THNS yields did not demonstrate faster removal compared to DOC in the Delta but reflected rapid removal in Suisun Bay and fresh input in the Bay with

continued removal. Record low flow in 2015 had high neutral sugar yields in the riverine endmembers and upper Delta and reflected removal of THNS in the Delta and Suisun Bay, lower THNS yields in the Bay, and a fresh input of terrestrial DOM before the marine endmember that caused 2015 to have a surge in THNS yield at the endmember compared to the Bay station.

Amino acid yields were higher in higher flow regime than the low flow (2016) which was characterized by low THAA yields with localized hotspots in the Delta. THAA yields in the record low flow were more similar to the high flow in 2014 than the low flow in 2016 and demonstrated variability within the estuary and enrichment in the riverine endmembers. Overall, THAA yields were low in the Bay across all flow regimes and reflected variability in the Delta and connection through Suisun Bay with flow regime.

THNS carbon-normalized yields were higher in the Delta than in the Bay even under different hydrological conditions. THAA carbon-normalized yields in most Delta-Bay sites were similar to yields measured in the incubation samples. THAA carbon-normalized yields were higher than incubation yields in some transect sites for all three years and were influenced by localized dynamics. Discharge from freshwater sources and in situ production did not show large variations in the percentage of neutral sugars in the Delta-Bay organic carbon, indicating a significant portion of the riverine DOM in this system is composed of refractory terrestrial DOM (Stepanauskas et al., 2005). Compositionally, neutral sugar abundances in all the transects were the same, which indicates extensive degradation already occurred before terrestrial DOM entered the system. Composition of the amino acids varied throughout the transects and seemed influenced by localized dynamics and seasonal variance as opposed to estuarine processes, which is likely variable due to source and diagenetic processing (Table 15, 16, 17). D-AA carbon-normalized concentrations showed microbial processing was more apparent in the bay during high flow than in the Delta while during record low it was present in hotspots in the Delta and Bay, and during normal low flow (2015), it was present in all sections of the estuary.

Principal component analysis of neutral sugars showed distinct compositional differences in the incubations (grasses, cattails, and tule versus pine and oak) and in the transects from the incubations (Figure 16). Principal component 1 (PC1) projects diagenetic alteration (Dauwe and Middelburg, 1998). With diagenesis, the abundance of neutral sugars shifted from Glc and Xyl to Fuc (Figure 16). Enrichment in fucose abundance increased with the shift from terrestrial DOM to microbial DOM, as mentioned in section 4.2 (Aspinall, 1983; Moers and Larter, 1993). Fucose is also an indicator of autochthonous production due to its abundance in algae or brown seaweed (Aspinall, 1983). All transects were enriched in Fuc reflecting extensive decomposition. There was no compositional distinction in the neutral sugars of the three transects. Diagenesis of the riverine DOM occurred before the DOM reached the Delta-Bay system in all three transects. The PC2 variable could describe source. In section 4.2, the distinct THNS composition in the incubations was discussed. Grasses, cattails, and tule were enriched in xylose while pine and oak were enriched in glucose. The PCA of THNS suggested DOM collected in the transects showed inputs from grasses, tule, cattails, or other wetlands origin as opposed to oak and pine, and further decomposition of the vascular plant leachates would merge the individual leachates towards the heavily degraded transects.

The principal component analysis of THAA molar abundance in the transects and incubations did not yield any clues on potentials sources for DOM in transect samples (Figure 16). Transects were separated along the PC1 axis. Gly is an indicator of decomposition, and was enriched in the 2015 transect but not in the 2016 transect. Variable degrees of in-situ production and associated input of amino acid-rich phytoplankton DOM could explain the observed trends in amino acid composition.

Studies in multiple systems around the globe have been conducted on the impact of photochemical transformations on DOM with two opposing observances of this impact (Kieber et al., 1989; Lindell et al., 1995; Amon and Benner, 1996; Benner and Biddanda, 1998; Obernosterer et al., 1999; Moran et al., 2000; Miller et al., 2002; Stepanauskas et al., 2005). Studies have determined previously refractory DOM can be

transformed into readily biolabile DOM after photochemical processing occurs (Kieber et al., 1989; Moran et al., 2000; Miller et al., 2002). Decreasing bioavailability of DOM after it has undergone photochemical transformations has also been observed (Amon and Benner, 1996; Benner and Biddanda, 1998; Obernosterer et al., 1999). Using DOC bioavailability assays, Stepanauskas et al. (2005) determined ~10% of DOC in the Delta is bioavailable and rapidly consumed in the Delta with the rest being terrestrial and primarily refractory throughout the year due to residence times in the system and interactions with organic-rich soils.

THNS carbon-normalized yields of vascular plant leachate during incubations in this experiment demonstrated the potential to utilize THNS yields as an indicator of boilable terrestrial DOC (tDOC). Due to the high neutral sugar content in the organic carbon of incubated leachates coupled with low amino acid content, it was possible to apply Davis and Benner (2007) equations to calculate the labile fraction of both tDOC and in situ DOC in the Delta-Bay system. THNS carbon-normalized yields were used to calculate the labile fraction of tDOC in the transect samples. Leachate DOC in our incubations had very low amino acid content, so THAA carbon-normalized yields were used to calculate the labile fraction of in situ DOC.

The labile fraction of DOC ranged 0 to 61% total labile DOC in the Delta (Figure 17) with higher total labile DOC values in the Vernalis and Garcia Bend sampling sites in 2015, which reflects Stepanauskas' et al. (2005) findings of higher biolabile DOC at Vernalis than in the Delta. Labile tDOC values in our transect samples ranged from 0 to 36% in the Delta and in localized stations were higher than the range (~6-16 %) provided by Stepanauskas et al. (2005). Differences in labile DOC through comparison to Stepanauskas et al. (2005) values and comparison between the 2014, 2015, and 2016 transects analyzed in this study can be contributed to the complexity of this system. Riverine DOM in this system is heterogenic and derived from varying sources (terrestrial runoff, in situ derived, and wetland runoff) that is highly localized in the estuary. The absence of a labile fraction gradient across the Delta to the Bay reflected the rapid rework of the labile component of riverine DOM under the dynamics of this

system. Depleted to low in situ DOC in the Bay for all three transects revealed microbial processing was not as significant in the Bay as in the Delta. Continued removal of aromaticity during high flow suggests the Bay is driven by photochemical processing. Renewed (labile) tDOC in the Bay during low flow in 2016 can explain the higher aromaticity (~13% OC) seen in the 2016 transect.

Furthermore, Stepanauskas et al. (2005) found solar radiation impacted DOC bioavailability negatively potentially due to phototransformation of labile DOC to refractory organic constituents. Despite allochthonous DOM dominance in riverine and estuarine systems, it has been suggested that autochthonous organic matter is an important biolabile pool for bacterial and phytoplankton production in estuarine and riverine systems (McCallister et al., 2006 and references therein). Eckard et al. (2007) also found in situ production had a similar impact to DOC concentrations in the Delta-Bay system as riverine DOM from the Sacramento and San Joaquin Rivers. Therefore, in situ DOM potentially could significantly impact the concentration, composition, and ultimately the fate of the DOM in the Delta-Bay system.

The Sacramento-San Joaquin River Delta and San Francisco Bay estuary experiences drastic seasonal regime flow between the winter and summer seasons (California Department of Water Resources, Dayflow, 2017). Neutral sugar yields in the riverine endmembers were similar (~4-5% OC) during the high flow regime and the low flow and were elevated (~8% OC) in the record low flow measured in 2015. THNS yields at the marine endmembers were similar across all flow regimes and reflected removal of labile tDOC. Amino acid yields were enriched in riverine endmembers collected during the record low flow compared to the high and low flows (Table 16).The marine endmember was enriched in THAA yields during the high flow and the record low flow, while the low flow regime was depleted in THAA yields. Higher carbon-normalized D-AA concentrations for the San Joaquin River endmember and the Sacramento River endmember in the record low flow (67 and 161 nmol mgC^{-1} respectively) than in the high flow (39 and 26 nmol mgC^{-1} respectively) or low flow (15

and 27 nmol mgC^{-1} respectively) reflected autochthonous input of DOM in the rivers was spurred under the conditions in the 2015 transect.

Source inputs during extreme low flow were specific to highly labile DOM with not only high in situ labile fractions in the rivers but also high tDOC fractions that suggest fresher terrestrial input of DOC than during high riverine discharge. During higher riverine discharge, DOC concentrations were much higher in the riverine endmembers and contain a larger component of semi-labile or refractory DOM than inputs in the record low flow. The labile fraction of tDOC was greater than the labile fraction of in situ DOC during both high and low flow regimes, but during the record low flow observed in 2015, the in situ labile fraction of DOC was greater in the Sacramento River than the tDOC labile fraction. This suggests that between the standard flow regimes, high flow delivers more labile tDOC and favors autochthonous inputs of DOC more than low flow conditions, but extreme low flow conditions favor autochthonous inputs of DOM in the rivers where increased residence time coupled with terrestrial DOM that has a larger labile fraction encourages autochthonous production of DOM.

Comparison of the two riverine endmembers (Vernalis and Garcia Bend) did not yield many source-derived compositional differences in the DOM. Since compositional differences in DOM are influenced in part by source, during a large discharge event such as the transect samples collected in December of 2014, DOM samples would be comprised of terrestrial DOM that would bare indicators of its origin. Since the Sacramento River is surrounded by agricultural lands, the difference in input vegetation from the Sacramento River and the San Joaquin could be compositionally visible in the leached DOM flushed into the river and collected at the river endmembers. However, comparison of the Vernalis site to the Garcia Bend site in the 2014 transect revealed no significant compositional differences in the amino acids and neutral sugars in the two rivers. In contrast, there were more compositional differences in the two riverine endmembers in the summer transects when less discharge occurred and in situ production increased, reflected in amino acid carbon-normalized concentrations, carbon-

normalized D-AA concentrations, and the principal component analysis of the amino acid compositions.

5. CONCLUSION

Global riverine discharge delivers 0.20-0.36 PgC per year to ocean reservoirs (Schlesinger and Melack, 1981; Meybeck 1982, 1993; Ludwig et al., 1996; Hedges et al., 1997; Aitkenhead and McDowell, 2000; Cauwet, 2002; Dai et al., 2012). Terrestrial DOM is a large component of riverine DOM and serves as a major source of metabolic energy to microorganisms. Extensive processing of terrestrial DOM in rivers and estuarine systems leads to small contributions to marine DOM (Opsahl and Benner, 1997). The processing of terrestrial DOM in estuarine systems is difficult to understand due to multiple potential sources of DOM and variability in composition that influences processing in these systems. Therefore, investigation into the processes terrestrial DOM undergoes in estuarine systems can provide insight in compositional changes that ultimately determine the fate of DOM.

Coupled incubation experiments of vascular plant leachates revealed large initial losses in the available DOC as well as amino acids and neutral sugars. Comparison of the five types of vascular plants used in incubations revealed distinct DOM compositions based on source and variability in the rate of decay of DOM components. Preferential degradation of neutral sugars in the leachates was reflected in high decay rate constants (0.065-0.463 $days^{-1}$) for THNS in each leachate. The large percentage of DOC composed of neutral sugars in vascular plant leachate DOM enabled the use of neutral sugars as an indicator of degradation. Carbon-normalized yields of neutral sugars were a large component of fresher leachate material that was preferentially degraded while carbon-normalized yields of amino acids were a smaller component of the DOC in vascular plant leachates.

Coupled photochemical-microbial incubations provided biomarker tools to elucidate sources and transformation reactions of DOM in the Delta and Bay system. We concluded that watershed characteristics, dominant vegetation, extent of wetland area and other environmental characteristics of the Delta-Bay were the most important factors influencing the composition of riverine DOM. Differences in DOM compositions and

concentrations related to differences in regions, highlighting heterogenetic inputs, hydrology of the system, and in situ production. Furthermore, terrestrial DOM was extensively degraded prior to entering the Delta.

A conceptual model is presented in Fig. 18 to summarize major processes occurring in the Sacramento-San Joaquin River Delta and San Francisco Bay estuary. The Delta section is strongly influenced by terrestrial DOM leached from vascular plant litter, soil horizons and microbially-derived DOM. Terrestrial DOM sources varied with season and flow regime. DOM transformations in the Delta section were primarily due to microbial processes.

DOM between the end of the Delta and into Suisun Bay still bears a strong signal of terrestrial DOM delivered from the river delta. There, riverine discharge meets tidally influenced saltwater creating ephemeral pockets with high in situ productivity and DOM production, especially in summer during low flow. Similar to the Delta, DOM decomposition is primarily driven by microbial processes.

The San Francisco Bay system shows contributions of remaining DOM delivered from the Delta and attenuated through Suisan Bay, and DOM derived from in situ production. As water clarity and associated light penetration increases, photochemical as well as microbial reactions lead to decomposition and transformations of DOM.

Overall, the efficient removal of DOM delivered from the rivers along the path through Suisun Bay and San Francisco Bay demonstrates that this estuarine system acts as an efficient “filter” and sink of terrestrial DOM. The efficient mineralization of terrestrial DOM dominated by microbial processes suggests a major control on air-sea CO_2 fluxes, acidification and nutrient budgets in estuaries.

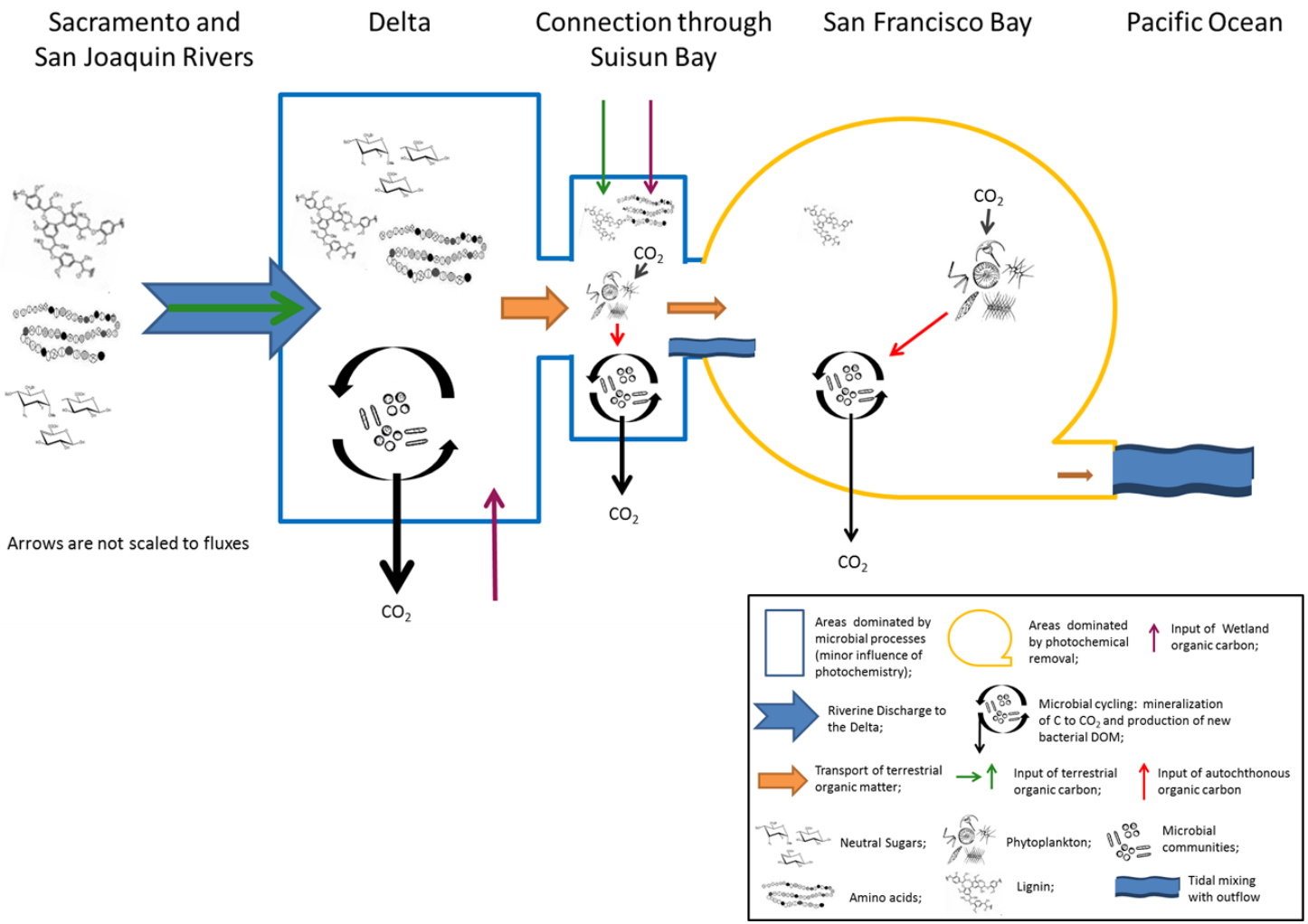

Figure 18 Description of the organic matter inputs, processing, and transformations that occur in the Sacramento-San Joaquin River Delta and San Francisco Bay estuary.

REFERENCES

Aitkenhead, J. A., & McDowell, W. H. (2000). Soil C: N ratio as a predictor of annual riverine DOC flux at local and global scales. *Global Biogeochemical Cycles, 14*(1), 127-138.

Amon, R. M., & Benner, R. (1996). Bacterial utilization of different size classes of dissolved organic matter. *Limnology and Oceanography, 41*(1), 41-51.

Amon, R. & Benner, R. (2003). Combined neutral sugars as indicators of the diagenetic state of dissolved organic matter in the Arctic Ocean. *Deep Sea Research Part I: Oceanographic Research Papers,* 50**,** 151-169.

Amon, R., Fitznar, H.-P., & Benner, R. (2001). Linkages among the bioreactivity, chemical composition, and diagenetic state of marine dissolved organic matter. *Limnology and Oceanography,* 46**,** 287-297.

Aspinall, G. (1970). Pectins, plant gums, and other plant polysaccharides. *The Carbohydrates: Chemistry and Biochemistry.* Elsevier Inc.

Aspinall, G. O. (1983). The polysaccharides. *The Polysaccharides*, *2*. Elsevier Inc.

Benner, R., Moran, M. A., & Hodson, R. E. (1986). Biogeochemical cycling of lignocellulosic carbon in marine and freshwater ecosystems: Relative contributions of procaryotes and eucaryotes. *Limnology and Oceanography, 31*(1), 89-100.

Benner, R., & Biddanda, B. (1998). Photochemical transformations of surface and deep marine dissolved organic matter: Effects on bacterial growth. *Limnology and Oceanography, 43*(6), 1373-1378.

Benner, R. & Opsahl, S. (2001). Molecular indicators of the sources and transformations of dissolved organic matter in the Mississippi river plume. *Organic Geochemistry, 32(4),* 597-611.

Benner, R. & Kaiser, K. (2003). Abundance of amino sugars and peptidoglycan in marine particulate and dissolved organic matter. *Limnology and Oceanography,* 48**,** 118-128.

Benner, R. & Kaiser, K. (2011). Biological and photochemical transformations of amino acids and lignin phenols in riverine dissolved organic matter. *Biogeochemistry*, *102*, 209-222.

Bianchi, T. S. & Canuel, E. A. (2011). *Chemical Biomarkers in Aquatic Ecosystems.* Princeton University Press.

Bianchi, T. S., Filley, T., Dria, K., & Hatcher, P. G. (2004). Temporal variability in sources of dissolved organic carbon in the lower Mississippi River. *Geochimica et Cosmochimica Acta*, *68*(5), 959-967.

Birdwell, J. E., & Engel, A. S. (2010). Characterization of dissolved organic matter in cave and spring waters using UV–Vis absorbance and fluorescence spectroscopy. *Organic Geochemistry*, *41*(3), 270-280.

Boyer, E. W., Hornberger, G. M., Bencala, K. E., & McKnight, D. M. (1997). Response characteristics of DOC flushing in an alpine catchment. *Hydrological Processes*, *11*(12), 1635-1647.

Burns, K. A., Brunskill, G., & Brinkman, D. (2008). Organic carbon and nutrient fluxes to the coastal zone from the Sepik River outflow. *Continental Shelf Research*, *28*, 283-301.

California Department of Water Resources. Dayflow data. Accessed December 12, 2016. http://www.water.ca.gov/dayflow/

Carlson, C. A., & Hansell, D. A. (2014). DOM sources, sinks, reactivity, and budgets. In *Biogeochemistry of Marine Dissolved Organic Matter: Second Edition*. Elsevier Inc.

Cauwet, G. (2002). DOM in the coastal zone. *Biogeochemistry of Marine Dissolved Organic Matter: Second Edition*, 579-609. Elsevier Inc.

Cherrier, J. & Bauer, J. E. (2004). Bacterial utilization of transient plankton-derived dissolved organic carbon and nitrogen inputs in surface ocean waters. *Aquatic Microbial Ecology*, *35*(3), 229-241.

Childers, D. L., Day, J. W., & Mckellar, H. N. (2000). Twenty More Years of Marsh and Estuarine Flux Studies: Revisiting Nixon (1980). In M. P. Weinstein & D. A.

Kreeger (Eds.), *Concepts and Controversies in Tidal Marsh Ecology*, 391-423. Springer Netherlands.

Cloern, J. E., & Dufford, R. (2005). Phytoplankton community ecology: principles applied in San Francisco Bay. *Marine Ecology Progress Series*, *285*, 11-28.

Coble, P. (2007). Marine optical biogeochemistry: the chemistry of ocean color. *Chemical Reviews*, *107*(2), 402–418.

Coffin, R. B. (1989). Bacterial uptake of dissolved free and combined amino acids in estuarine waters. *Limnology and Oceanography*, *34*(3), 531-542.

Cory, R. M., & McKnight, D. M. (2005). Fluorescence spectroscopy reveals ubiquitous presence of oxidized and reduced quinones in dissolved organic matter. *Environmental Science & Technology*, *39*(21), 8142-8149.

Cory, R. M., Ward, C. P., Crump, B. C., & Kling, G. W. (2014). Sunlight controls water column processing of carbon in arctic fresh waters. *Science*, *345*(6199), 925-928.

Cowie, G. L. & Hedges, J. I. (1984). Determination of neutral sugars in plankton, sediments, and wood by capillary gas chromatography of equilibrated isomeric mixtures. *Analytical Chemistry, 56*, 497-504.

Cowie, G. L., & Hedges, J. I. (1994). Biochemical indicators of diagenetic alteration in natural organic matter mixtures. *Nature, 369*(6478), 304-307.

Dai, M., Yin, Z., Meng, F., Liu, Q., & Cai, W. J. (2012). Spatial distribution of riverine DOC inputs to the ocean: an updated global synthesis. *Current Opinion in Environmental Sustainability*, *4*(2), 170-178.

Dauwe, B. & Middelburg, J. J. (1998). Amino acids and hexosamines as indicators of organic matter degradation state in North Sea sediments. *Limnology and Oceanography, 43***,** 782-798.

Davis, J. & Benner, R. (2007). Quantitative estimates of labile and semi-labile dissolved organic carbon in the western Arctic Ocean: A molecular approach. *Limnology and Oceanography*, *52*(6), 2434-2444.

Davis, S. E., Childers, D. L., & Noe, G. B. (2006). The contribution of leaching to the rapid release of nutrients and carbon in the early decay of wetland vegetation. *Hydrobiologia*, *569*(1), 87-97.

Davis, J., Kaiser, K., & Benner, R. (2009). Amino acid and amino sugar yields and compositions as indicators of dissolved organic matter diagenesis. *Organic Geochemistry*, *40*(3), 343-352.

De Saussure, N. T. (1804). *Recherches Chimiques Sur la Végétation*. Chez la Ve. Nyon.

Dighton, J., & Boddy, L. (1989). Role of fungi in nitrogen, phosphorus and sulphur cycling in temperate forest ecosystems. *Cambridge University Press*, 267–298.

Dittmar, T. & Paeng, J. (2009). A heat-induced molecular signature in marine dissolved organic matter. *Nature Geoscience*, *2*(3), 175–179.

Dittmar, T., Fitznar, H. P., & Kattner, G. (2001). Origin and biogeochemical cycling of organic nitrogen in the eastern Arctic Ocean as evident from D-and L-amino acids. *Geochimica et Cosmochimica Acta*, *65***,** 4103-4114.

Druffel, E., Williams, PM, & Bauer, JE. (1992). Cycling of dissolved and particulate organic matter in the open ocean. *Journal of Geophysical Research*, *97*(C10), 15,639-15,659.

Eckard, R. S., Hernes, P. J., Bergamaschi, B. A., Stepanauskas, R., & Kendall, C. (2007). Landscape scale controls on the vascular plant component of dissolved organic carbon across a freshwater delta. *Geochimica et Cosmochimica Acta*, *71*(24), 5968-5984.

Enright, C., & Culberson, S. D. (2009). Salinity trends, variability, and control in the northern reach of the San Francisco Estuary. *San Francisco Estuary and Watershed Science*, *7*(2).

Fellman, J. B., Hood, E., & Spencer, R. G. (2010). Fluorescence spectroscopy opens new windows into dissolved organic matter dynamics in freshwater ecosystems: A review. *Limnology and Oceanography*, *55*(6), 2452-2462.

Fichot, C. G. & Benner, R. (2011). A novel method to estimate DOC concentrations from CDOM absorption coefficients in coastal waters. *Geophysical Research Letters*, *38*(3).

Fichot, C. G., & Benner, R. (2012). The spectral slope coefficient of chromophoric dissolved organic matter (S275–295) as a tracer of terrigenous dissolved organic carbon in river-influenced ocean margins. *Limnology and Oceanography*, *57*(5), 1453-1466.

Fichot, C. G. & Benner, R. (2014). The fate of terrigenous dissolved organic carbon in a river-influenced ocean margin. *Global Biogeochemical Cycles*, *28*(3), 300-318.

Fichot, C. G., Benner, R., Kaiser, K., Shen, Y., Amon, R. M., Ogawa, H., & Lu, C. J. (2016). Predicting dissolved lignin phenol concentrations in the coastal ocean from chromophoric dissolved organic matter (CDOM) absorption coefficients. *Frontiers in Marine Science*, *3*, 7.

Fox, J. P., Mongan, T. R., & Miller, W. J. (1990). Trends in Freshwater Inflow to San Francisco Bay from the Sacramento-San Joaquin Delta. *JAWRA Journal of the American Water Resources Association*, *26*(1), 101-116.

Frey, K. E. & Smith, L. C. (2005). Amplified carbon release from vast West Siberian peatlands by 2100. *Geophysical Research Letters*, *32*(9).

Fukushima, M., Tanabe, Y., Yabuta, H., Tanaka, F., Ichikawa, H., Tatsumi, K., & Watanabe, A. (2006). Water solubility enhancement effects of some polychlorinated organic pollutants by dissolved organic carbon from a soil with a higher organic carbon content. *Journal of Environmental Science and Health Part A*, *41*(8), 1483-1494.

Fuchs, G., Boll, M., & Heider, J. (2011). Microbial degradation of aromatic compounds—from one strategy to four. *Nature Reviews Microbiology*, *9*(11), 803-816.

Gourlay, C., Tusseau-Vuillemin, M. H., Mouchel, J. M., & Garric, J. (2005). The ability of dissolved organic matter (DOM) to influence benzo [a] pyrene bioavailability

increases with DOM biodegradation. *Ecotoxicology and Environmental Safety*, *61*(1), 74-82.

Gruber, D. F., Simjouw, J. P., Seitzinger, S. P., & Taghon, G. L. (2006). Dynamics and characterization of refractory dissolved organic matter produced by a pure bacterial culture in an experimental predator-prey system. *Applied and Environmental Microbiology*, *72*(6), 4184-4191.

Healey, M.C., Dettinger, M. D., and Norgaard, R. B. (2008). The State of Bay-Delta Science. Sacramento, CA: CALFED Science Program.

Hedges, J. I. (1992). Global biogeochemical cycles: progress and problems. *Marine Chemistry*, *39*(1-3), 67-93.

Hedges, J., Cowie, G. L., Richey, J. E., Quay, P. D., Benner, R., Strom, M., & Forsberg, B. R. (1994). Origins and processing of organic matter in the Amazon River as indicated by carbohydrates and amino acids. *Limnology and Oceanography*, *39*, 743-761.

Hedges, J. I., Keil, R. G., & Benner, R. (1997). What happens to terrestrial organic matter in the ocean? *Organic Geochemistry*, 27(5), 195-212.

Helms, J. R., Stubbins, A., Ritchie, J. D., Minor, E. C., Kieber, D. J., & Mopper, K. (2008). Absorption spectral slopes and slope ratios as indicators of molecular weight, source, and photobleaching of chromophoric dissolved organic matter. *Limnology and Oceanography*, *53*(3), 955-969.

Helms, J. R., Stubbins, A., Perdue, E. M., Green, N. W., Chen, H., & Mopper, K. (2013). Photochemical bleaching of oceanic dissolved organic matter and its effect on absorption spectral slope and fluorescence. *Marine Chemistry*, *155*, 81-91.

Hernes, P. J., & Benner, R. (2003). Photochemical and microbial degradation of dissolved lignin phenols: Implications for the fate of terrigenous dissolved organic matter in marine environments. *Journal of Geophysical Research: Oceans*, *108*(C9).

Hernes, P. J., Robinson, A. C., & Aufdenkampe, A. K. (2007). Fractionation of lignin during leaching and sorption and implications for organic matter "freshness". *Geophysical Research Letters, 34*.

Hernes, P. J., Spencer, R. G., Dyda, R. Y., Pellerin, B. A., Bachand, P. A., & Bergamaschi, B. A. (2008). The role of hydrologic regimes on dissolved organic carbon composition in an agricultural watershed. *Geochimica et Cosmochimica Acta, 72*(21), 5266-5277.

Holmes, R. M., Mcclelland, J. W., Peterson, B. J., Tank, S. E., Bulygina, E., Eglinton, T. I., Gordeev, V. V., Gurtovaya, T. Y., Raymond, P. A., & Repeta, D. J. (2012). Seasonal and annual fluxes of nutrients and organic matter from large rivers to the Arctic Ocean and surrounding seas. *Estuaries and Coasts, 35***,** 369-382.

Huguet, A., Vacher, L., Relexans, S., Saubusse, S., Froidefond, J. M., & Parlanti, E. (2009). Properties of fluorescent dissolved organic matter in the Gironde Estuary. *Organic Geochemistry, 40*(6), 706-719.

Hunter, Y. R., & Kuwabara, J. S. (1994). Ionic strength and DOC determinations from various freshwater sources to the San Francisco Bay. *Bulletin of Environmental Contamination and Toxicology, 52*(2), 311-318.

Ingebritsen S. E., Ikehara M. E., Galloway D. L., Jones D. R. (2000). Delta subsidence in California: the sinking heart of the state. U.S. Geological Survey, FS-005-00.

Jaffé, R., McKnight, D., Maie, N., Cory, R., McDowell, W. H., & Campbell, J. L. (2008). Spatial and temporal variations in DOM composition in ecosystems: The importance of long-term monitoring of optical properties. *Journal of Geophysical Research: Biogeosciences, 113*(G4).

Jassby, A. D., & Cloern, J. E. (2000). Organic matter sources and rehabilitation of the Sacramento-San Joaquin Delta (California, USA). *Aquatic Conservation: Marine and Freshwater Ecosystems,* 10, 323-352.

Jassby, A. D., Cloern, J. E., & Cole, B. E. (2002). Annual primary production: Patterns and mechanisms of change in a nutrient-rich tidal ecosystem. *Limnology and Oceanography, 47*(3), 698-712.

Jordan, T. E., & Correll, D. L. (1991). Continuous automated sampling of tidal exchanges of nutrients by brackish marshes. *Estuarine, Coastal and Shelf Science*, *32*(6), 527-545.

Jørgensen, N. O.G., Stepanaukas, R., Pedersen, A.-G. U., Hansen, M. and Nybroe, O. (2003). Occurrence and degradation of peptidoglycan in aquatic environments. *FEMS Microbiology Ecology, 46*, 269–280.

Kaiser, K. & Benner, R. (2000). Determination of amino sugars in environmental samples with high salt content by high-performance anion-exchange chromatography and pulsed amperometric detection. *Analytical Chemistry*, *72*(11), 2566-2572.

Kaiser, K. & Benner, R. (2005). Hydrolysis-induced racemization of amino acids. *Limnology and Oceanography Methods*, *3*, 318-325.

Kaiser, K. & Benner, R. (2008). Major bacterial contribution to the ocean reservoir of detrital organic carbon and nitrogen. *Limnology and Oceanography*, *53*(1), 99.

Kaiser, K. & Benner, R. (2009). Biochemical composition and size distribution of organic matter at the Pacific and Atlantic time-series stations. *Marine Chemistry, 113*(1), 63-77.

Kaiser, K., Benner, R., & Amon, R. M. W. (2016). The fate of terrigenous dissolved organic carbon on the Eurasian shelves and export to the North Atlantic. *Journal of Geophysical Research: Oceans, 122*(1), 4-22.

Kawasaki, N. & Benner, R. (2006). Bacterial release of dissolved organic matter during cell growth and decline: Molecular origin and composition. *Limnology and Oceanography*, *51*(5), 2170-2180.

Keil, R. G. & Kirchman, D. L. (1993). Dissolved combined amino acids: chemical form and utilization by marine bacteria. *Limnology and Oceanography*, *38*(6), 1256-1270.

Kieber, D. J., McDaniel, J., & Mopper, K. (1989). Photochemical source of biological substrates in sea water: Implications for carbon cycling. *Nature*, *341*, 19.

Kraus, T. E., Bergamaschi, B. A., Hernes, P. J., Spencer, R. G., Stepanauskas, R., Kendall, C., ... & Fujii, R. (2008). Assessing the contribution of wetlands and subsided islands to dissolved organic matter and disinfection byproduct precursors in the Sacramento–San Joaquin River Delta: a geochemical approach. *Organic Geochemistry*, *39*(9), 1302-1318.

Kuwabara, J. S., & Luther, G. W. (1993). Dissolved sulfides in the oxic water column of San Francisco Bay, California. *Estuaries and Coasts*, *16*(3), 567-573.

Lindell, M. J., Granéli, W., & Tranvik, L. J. (1995). Enhanced bacterial growth in response to photochemical transformation of dissolved organic matter. *Limnology and Oceanography*, *40*(1), 195-199.

Loh, A. N., Bauer, J. E., & Druffel, E. (2004). Variable ageing and storage of dissolved organic components in the open ocean. *Nature*, *430*, 877-881.

Ludwig, W., Probst, J. L., & Kempe, S. (1996). Predicting the oceanic input of organic carbon by continental erosion. *Global Biogeochemical Cycles*, *10*(1), 23-41.

Maie, N., Jaffe, R., Myoshi, M., and Childers, D. (2006). Quantitative and qualitative aspects of dissolved organic carbon leached from senescent plants in an oligotrophic wetland. *Biogeochemistry, 78*, 285–314.

Mannino, A., & Harvey, H. (2000). Biochemical composition of particles and dissolved organic matter along an estuarine gradient: Sources and implications for DOM reactivity. *Limnology and Oceanography*, *45*(4), 775–788.

McCallister, S. L., Bauer, J. E., Ducklow, H. W., & Canuel, E. A. (2006). Sources of estuarine dissolved and particulate organic matter: a multi-tracer approach. *Organic Geochemistry*, *37*(4), 454-468.

McDowell, W.H. and G.E. Likens (1988). Origin, composition, and flux of dissolved organic-carbon in the Hubbard Brook Valley. *Ecological Monographs, 58*(3), 177-195.

McGlynn, B. L., & McDonnell, J. J. (2003). Role of discrete landscape units in controlling catchment dissolved organic carbon dynamics. *Water Resources Research*, *39*(4).

McKnight, D. M., Boyer, E. W., Westerhoff, P. K., Doran, P. T., Kulbe, T., & Andersen, D. T. (2001). Spectrofluorometric characterization of dissolved organic matter for indication of precursor organic material and aromaticity. *Limnology and Oceanography, 46*(1), 38-48.

Meybeck, M. (1982). Carbon, nitrogen, and phosphorus transport by world rivers. *American Journal of Science, 282***,** 401-450.

Meybeck, M. (1993). Riverine transport of atmospheric carbon: sources, global typology and budget. *Water, Air, and Soil Pollution, 70*(1), 443-463.

Miller, W. L., & Moran, M. A. (1997). Interaction of photochemical and microbial processes in the degradation of refractory dissolved organic matter from a coastal marine environment. *Limnology and Oceanography,* 42(6), 1317-1324.

Miller, W. L., & Zepp, R. G. (1995). Photochemical production of dissolved inorganic carbon from terrestrial organic matter: Significance to the oceanic organic carbon cycle. *Geophysical Research Letters, 22*(4), 417-420.

Miller, W. L., Moran, M., Sheldon, W. M., Zepp, R. G., & Opsahl, S. (2002). Determination of apparent quantum yield spectra for the formation of biologically labile photoproducts. *Limnology and Oceanography, 47*(2), 343-352.

Moers, M. E. C., & Larter, S. R. (1993). Neutral monosaccharides from a hypersaline tropical environment: Applications to the characterization of modern and ancient ecosystems. *Geochimica et Cosmochimica Acta*, *57*(13), 3063-3071.

Mopper, K., & Kieber, D. J. (2002). Photochemistry and the cycling of carbon, sulfur, nitrogen and phosphorus. *Biogeochemistry of Marine Dissolved Organic Matter: Second Edition* (455-507). Elsevier Inc.

Mopper, K., & Schultz, C. A. (1993). Fluorescence as a possible tool for studying the nature and water column distribution of DOC components. *Marine Chemistry, 41*(1-3), 229-238.

Mopper, K., & Stahovec, W. L. (1986). Sources and sinks of low molecular weight organic carbonyl compounds in seawater. *Marine Chemistry, 19*(4), 305-321.

Mopper, K., Zhou, X., Kieber, R. J., Kieber, D. J., Sikorski, R. J., & Jones, R. D. (1991). Photochemical degradation of dissolved organic carbon and its impact on the oceanic carbon cycle. *Nature, 353***,** 60-62.

Moran, M. A., Sheldon, W. M., & Zepp, R. G. (2000). Carbon loss and optical property changes during long-term photochemical and biological degradation of estuarine dissolved organic matter. *Limnology and Oceanography*, *45*(6), 1254-1264.

Murrell, M. C., & Hollibaugh, J. T. (2000). Distribution and composition of dissolved and particulate organic carbon in northern San Francisco Bay during low flow conditions. *Estuarine, Coastal and Shelf Science*, *51*(1), 75-90.

Neff, J., Finlay, J., Zimov, S., Davydov, S., Carrasco, J., Schuur, E., & Davydova, A. (2006). Seasonal changes in the age and structure of dissolved organic carbon in Siberian rivers and streams. *Geophysical Research Letters, 33*(23).

Nixon, S. W. (1980). Between coastal marshes and coastal waters—a review of twenty years of speculation and research on the role of salt marshes in estuarine productivity and water chemistry. In P. Hamilton & K. B. Macdonald (Eds.), *Estuarine and Wetland Processes: With Emphasis on Modeling* (pp. 437-525). Boston, MA: Springer US.

Nykvist, N. (1963) Leaching and decomposition of water-soluble organic substances from different types of leaf and needle litter, *Studia Forestalia Suecica*, *3*, 1-31.

Obernosterer, I., Reitner, B., & Herndl, G. J. (1999). Contrasting effects of solar radiation on dissolved organic matter and its bioavailability to marine bacterioplankton. *Limnology and Oceanography*, *44*(7), 1645-1654.

Obernosterer, I. & Benner, R. (2004). Competition between biological and photochemical processes in the mineralization of dissolved organic carbon. *Limnology and Oceanography*, *49*(1), 117-124.

Oh, N. H., Pellerin, B. A., Bachand, P. A., Hernes, P. J., Bachand, S. M., Ohara, N., ... & Horwath, W. R. (2013). The role of irrigation runoff and winter rainfall on dissolved organic carbon loads in an agricultural watershed. *Agriculture, Ecosystems & Environment*, *179*, 1-10.

Ohno, T. (2002). Fluorescence inner-filtering correction for determining the humification index of dissolved organic matter. *Environmental Science & Technology*, *36*(4), 742-746.

Opsahl, S., & Benner, R. (1993). Decomposition of senescent blades of the seagrass *Halodule wrightii* in a subtropical lagoon. *Marine Ecology Progress Series*, *94*, 191.

Opsahl, S., & Benner, R. (1997). Distribution and cycling of terrigenous dissolved organic matter in the ocean. *Nature*, *386*(6624), 480.

Opsahl, S., & Benner, R. (1998). Photochemical reactivity of dissolved lignin in river and ocean waters. *Limnology and Oceanography*, *43*(6), 1297-1304.

Opsahl, S., & Benner, R. (1999). Characterization of carbohydrates during early diagenesis of five vascular plant tissues. *Organic Geochemistry*, *30*(1), 83-94.

Osburn, C. L., Morris, D. P., Thorn, K. A., & Moeller, R. E. (2001). Chemical and optical changes in freshwater dissolved organic matter exposed to solar radiation. *Biogeochemistry*, *54*(3), 251-278.

Paulsen, S. C. (1997). A study of the mixing of natural flows using ICP-MS and the elemental composition of waters. Doctoral dissertation, California Institute of Technology.

Pèrez, M. T., Pausz, C., & Herndl, G. J. (2003). Major shift in bacterioplankton utilization of enantiomeric amino acids between surface waters and the ocean's interior. *Limnology and Oceanography*, *48*(2), 755-763.

Raymond, P. A., & Bauer, J. E. (2001). Use of 14 C and 13 C natural abundances for evaluating riverine, estuarine, and coastal DOC and POC sources and cycling: a review and synthesis. *Organic Geochemistry*, *32*(4), 469-485.

Roach, K. A. (2013). Environmental factors affecting incorporation of terrestrial material into large river food webs. *Freshwater Science*, *32*(1), 283-298.

Royer, T. V., & David, M. B. (2005). Export of dissolved organic carbon from agricultural streams in Illinois, USA. *Aquatic Sciences-Research Across Boundaries*, *67*(4), 465-471.

Said-Pullicino, D., Kaiser, K., Guggenberger, G., & Gigliotti, G. (2007). Changes in the chemical composition of water-extractable organic matter during composting: Distribution between stable and labile organic matter pools. *Chemosphere*, *66*(11), 2166-2176.

Sañudo-Wilhelmy, S. A., Rivera-Duarte, I., & Flegal, A. R. (1996). Distribution of colloidal trace metals in the San Francisco Bay estuary. *Geochimica et Cosmochimica Acta*, *60*(24), 4933-4944.

Santschi, P. H., Lenhart, J. J., & Honeyman, B. D. (1997). Heterogeneous processes affecting trace contaminant distribution in estuaries: the role of natural organic matter. *Marine Chemistry*, *58*(1), 99-125.

Schemel, L. E. (1984). Salinity, alkalinity, and dissolved and particulate organic carbon in the Sacramento River water at Rio Vista, California, and at other locations in the Sacramento-San Joaquin Delta. US Geological Survey.

Schlesinger, W., & Melack, J. (1981). Transport of organic carbon in the world's rivers. *Tellus*, *33*(2), 172–187.

Sinsabaugh, R. L., & Liptak, M. A. (1997). Enzymatic conversion of plant biomass. *The Mycota*, *4*, 347-57.

Skoog, A., & Benner, R. (1997). Aldoses in various size fractions of marine organic matter: Implications for carbon cycling. *Limnology and Oceanography*, *42*(8), 1803-1813.

Sleighter, R. L., & Hatcher, P. G. (2008). Molecular characterization of dissolved organic matter (DOM) along a river to ocean transect of the lower Chesapeake Bay by ultrahigh resolution electrospray ionization Fourier transform ion cyclotron resonance mass spectrometry. *Marine Chemistry*, *110*(3), 140-152.

Sommer, T., Suits, B., Mierzwa, M., & Wilde, J. (2006). Evaluation of residence time and entrainment using a particle tracking model for the Sacramento-San Joaquin Delta. Sacramento, CA: State of California, Department of Water Resources.

Spencer, R. G., Pellerin, B. A., Bergamaschi, B. A., Downing, B. D., Kraus, T. E., Smart, D. R., ... & Hernes, P. J. (2007). Diurnal variability in riverine dissolved

organic matter composition determined by in situ optical measurement in the San Joaquin River (California, USA). *Hydrological Processes*, *21*(23), 3181-3189.

Spencer, R. G., Aiken, G. R., & Wickland, K. P. (2008). Seasonal and spatial variability in dissolved organic matter quantity and composition from the Yukon River basin, Alaska. *Global Biogeochemical Cycles*, *22*(4).

Spencer, R. G., Aiken, G. R., Butler, K. D., Dornblaser, M. M., Striegl, R. G., & Hernes, P. J. (2009). Utilizing chromophoric dissolved organic matter measurements to derive export and reactivity of dissolved organic carbon exported to the Arctic Ocean: A case study of the Yukon River, Alaska. *Geophysical Research Letters*, *36*(6).

Stepanauskas, R., Moran, M. A., Bergamaschi, B. A., & Hollibaugh, J. T. (2005). Sources, bioavailability, and photoreactivity of dissolved organic carbon in the Sacramento–San Joaquin River Delta. *Biogeochemistry*, *74*(2), 131-149.

Stedmon, C., Amon, R., Rinehart, A., & Walker, S. (2011). The supply and characteristics of colored dissolved organic matter (CDOM) in the Arctic Ocean: Pan Arctic trends and differences. *Marine Chemistry, 124***,** 108-118.

Stubbins, A. (2001). Aspects of aquatic CO photoproduction from CDOM. PhD. thesis, New Castle Upon Tyne University.

Stubbins, A., Spencer, R., Chen, H., Hatcher, P., Mopper, K., Hernes, P., … Six, J. (2010). Illuminated darkness: Molecular signatures of Congo River dissolved organic matter and its photochemical alteration as revealed by ultrahigh precision mass spectrometry. *Limnology and Oceanography*, *55*(4), 1467–1477.

Tremblay, L. & Benner, R. (2009). Organic matter diagenesis and bacterial contributions to detrital carbon and nitrogen in the Amazon River system. *Limnology and Oceanography*, *54*(3), 681-691.

Tukey Jr, H. B. (1970). The leaching of substances from plants. *Annual Review of Plant Physiology*, *21*(1), 305-324.

Tzortziou, M., Neale, P. J., Megonigal, J. P., Pow, C. L., & Butterworth, M. (2011). Spatial gradients in dissolved carbon due to tidal marsh outwelling into a Chesapeake Bay estuary. *Marine Ecology Progress Series*, *426*, 41-56.

URS Corporation. (2007). Status and Trends of Delta-Suisun Services. Sacramento, CA: State of California, Department of Water Resources.

Vähätalo, A. V., & Wetzel, R. G. (2004). Photochemical and microbial decomposition of chromophoric dissolved organic matter during long (months–years) exposures. *Marine Chemistry*, *89*(1), 313-326.

Walker, S. A., Amon, R. M., & Stedmon, C. A. (2013). Variations in high-latitude riverine fluorescent dissolved organic matter: A comparison of large Arctic rivers. *Journal of Geophysical Research: Biogeosciences*, *118*(4), 1689-1702.

Walters, R. A., Cheng, R. T., & Conomos, T. J. (1985). Time scales of circulation and mixing processes of San Francisco Bay waters. *Hydrobiologia*, *129*, 13-36.

Weishaar, J. L., Aiken, G. R., Bergamaschi, B. A., Fram, M. S., Fujii, R., & Mopper, K. (2003). Evaluation of specific ultraviolet absorbance as an indicator of the chemical composition and reactivity of dissolved organic carbon. *Environmental Science & Technology*, *37*(20), 4702-4708.

Williams, B. L., and A. C. Edwards. 1993. Processes influencing dissolved organic nitrogen, phosphorus and sulphur in soils. *Chem. Ecol.*, *8*, 203-215.

Yamashita, Y., & Tanoue, E. (2003). Chemical characterization of protein-like fluorophores in DOM in relation to aromatic amino acids. *Marine Chemistry*, *82*(3), 255-271.

Zou, L., Wang, X. C., Callahan, J., Culp, R. A., Chen, R. F., Altabet, M. A., & Sun, M. Y. (2004). Bacterial roles in the formation of high-molecular-weight dissolved organic matter in estuarine and coastal waters: Evidence from lipids and the compound-specific isotopic ratios. *Limnology and Oceanography*, *49*(1), 297-302.

Zsolnay, A., Baigar, E., Jimenez, M., Steinweg, B., & Saccomandi, F. (1999). Differentiating with fluorescence spectroscopy the sources of dissolved organic matter in soils subjected to drying. *Chemosphere*, *38*(1), 45-50.